

Using ARMAX models to determine the drivers of 40-150 keV GOES electron fluxes

L. E. Simms^{1,2}, N. Yu. Ganushkina^{1,3}, M. van de Kamp³, M. W. Liemohn¹, S. Dubyagin³

¹University of Michigan, Ann Arbor, USA

²Department of Physics, Augsburg University, Minneapolis, USA

³Finnish Meteorological Institute, Helsinki, Finland

Key Points:

- Substorms, as measured by *AE*, are the strongest direct influence on 40-150 keV electron flux
- Of the possible indirect drivers *N*, *V*, *Bz* show fairly equal influence on flux
- An ARMAX model removes diurnal cyclicality and allows a more accurate assessment of the correlations

Corresponding author: L. Simms, laurasim@umich.edu

This is the author manuscript accepted for publication and has undergone full peer review but has not been through the copyediting, typesetting, pagination and proofreading process, which may lead to differences between this version and the [Version of Record](#). Please cite this article as [doi: 10.1029/2022JA030538](https://doi.org/10.1029/2022JA030538).

This article is protected by copyright. All rights reserved.

Abstract

We investigate the drivers of 40-150 keV hourly electron flux at geostationary orbit (GOES 13) using ARMAX (autoregressive moving average transfer function multiple regression) models which remove the confounding effect of diurnal cyclicality and allow assessment of each parameter independently. By taking logs of the variables, we create nonlinear models. While many factors show high correlation with flux in single variable analysis (substorms, ULF waves, solar wind velocity (V), pressure (P), number density (N) and electric field (E_y), IMF B_z , Kp , and $SymH$), ARMAX models show substorms are the dominant influence at 40-75 keV and over 20-12 MLT, with little difference seen between disturbed and quiet periods. The E_y influence is positive post-midnight, negative post-noon. Pressure shows a negative influence, strongest at 150 keV. ULF waves are a more modest influence than suggested by single variable correlation. Kp and $SymH$ show little effect when other variables are included. Using path analysis, we calculate the summed direct and indirect influences through the driving of intermediate parameters. Pressure shows a summed direct and indirect influence nearly half that of the direct substorm effect. N , V , and B_z , as indirect drivers, are equally influential. While simple correlation or neural networks can be used for flux prediction, neither can effectively identify drivers. Instead, consideration of physical influences, removing cycles that artificially inflate correlations, and controlling the effects of other parameters gives a clearer picture of which are most influential in this system.

Plain Language Summary

Satellites may experience damaging surface charging due to high energy electrons present in the radiation belts. In this study, we explore the various factors that may influence these electron populations. We use an ARMAX statistical model (autoregressive moving average transfer function) that removes the confounding effect of diurnal cyclicality and allows assessment of each variable independently of others. Substorms, which inject electrons into the magnetosphere, are found to be the strongest influence, with most of their effect seen near local midnight. The electric field and pressure of the solar wind also show moderate effects. Not all variables that show high single variable correlations retain this influence in multivariate analyses. Kp and $SymH$, two indices of geomagnetic activity are highly correlated with electron levels in the magnetosphere, but show little influence in models controlling for the effects of solar wind parameters. Identifying direct, physical drivers, removing cycles that artificially inflate correlations, and controlling the effects of other parameters using multiple regression (specifically, ARMAX) gives a clearer picture of which parameters are most influential in this system.

1 Introduction

Geostationary/geosynchronous orbit (GEO) is highly populated with active satellites (<http://www.unoosa.org/oosa/osoindex/>) that can experience damaging surface charging due to high energy electrons present in the radiation belts (e.g., Lam et al., 2012; Loto'aniu et al., 2015; Koons et al., 2000; Choi et al., 2011; Matéo-Vélez et al., 2018). These and other studies suggest that surface charging is a function of factors in the space environment, including solar and geomagnetic activity, electron and ion flux magnitudes, and particle energy spectrum hardness. Charging events may also be more likely when the satellite is in the Earth's shadow (eclipse). Surface charging events often occur when there are increased electron fluxes at 10 - 50 keV (kilo electronvolt), and < 100 keV electrons may be more responsible for the most rapid surface charging events than electrons at higher energies (Thomsen et al., 2013; Matéo-Vélez et al., 2018). The abundance of these electrons fluctuates on time scales of minutes and also shows high spatial variability over the magnetosphere. For this reason, daily/orbit averaging misses much of the behavior of these electrons. Moreover, even moderate storms are not necessary for electron enhance-

64 ments in this energy range, with many surface charging events detected during low to
65 moderate substorm activity and no direct dependence on substorm strength (Matéo-Vélez
66 et al., 2018; Ganushkina et al., 2021).

67 A better understanding of keV electron flux behavior is needed, including details
68 of how fluxes are driven and by what parameters. While a prediction model may hint
69 at the drivers and mechanisms, no matter how well it may forecast, it is not a valid tool
70 for effectively testing hypotheses about physical drivers. Hypothesis testing is best done
71 with statistical tools developed specifically for this. Regression is one such tool, with mul-
72 tiple regression being the more appropriate test when multiple drivers are being consid-
73 ered. (Confusingly, the least squares method used in regression can also be used to cre-
74 ate prediction models, but this should not be confused with hypothesis testing.) The AR-
75 MAX method (autoregressive moving average transfer functions), which we discuss be-
76 low, is a refinement of regression that allows the modelling of time series behavior be-
77 fore the testing of input parameters. This will reduce possible spurious correlations that
78 can occur if both dependent and independent variable time series cycle or trend simul-
79 taneously.

80 MeV (mega electronvolt) electron fluxes at GEO have been more extensively stud-
81 ied and may show high overall correlations with solar wind parameters when daily av-
82 eraged (e.g., Blake et al., 1997), although the hourly response may be much lower (Simms
83 et al., 2022). Solar wind speed is often cited as the most important driver (Paulikas &
84 Blake, 1979; Li et al., 2001), although the relationship is complex (Reeves et al., 2011)
85 and, for example, Lyatsky and Khazanov (2008) and Balikhin et al. (2011) have shown
86 that the solar wind density is more associated with MeV electron variations. The solar
87 wind electric field (E_y) also shows an association with MeV flux (Baker et al., 2019) (but
88 see Pulkkinen et al. (2016) for a discussion of how well the solar E_y maps to the mag-
89 netospheric convective currents). However, the direct influence of many solar wind drivers
90 on even MeV electron flux is still unclear, both because much of the solar wind influence
91 may not be direct but instead mediated by waves and electron injections following sub-
92 storms (e.g., Simms et al., 2018a), and because simple correlations of solar wind param-
93 eters with electrons may be inflated by common cycles and trends if these commonal-
94 ities are not removed via such methods as differencing transformation or ARMAX mod-
95 elling (Simms et al., 2022). For keV electrons, there are even fewer simple answers as to
96 which of the solar wind parameters drive their variations.

97 Fluxes of low energy electrons have been modeled with a first principle kinetic ap-
98 proach in several ring current simulations (e.g., Harel et al., 1981; Fok et al., 2014; Ganushk-
99 ina et al., 2014; Chen et al., 2015; Jordanova et al., 2016). These models are driven by
100 different sets of solar wind, IMF (Interplanetary Magnetic Field) parameters and geo-
101 magnetic indices but the drivers are predetermined. The first principle models cannot
102 define the driving parameters themselves.

103 Empirical models can determine correlates of electron flux energies from eVs to sever-
104 al MeVs using a variety of fitting techniques. Among them, (i) one of the earliest mod-
105 els, the NASA (National Aeronautics and Space Administration) radiation belt models
106 for electrons such as AE8 traditionally used to specify the average charged particle flux
107 for space missions (Vette, 1991), (ii) the improved AE9/SPM models (Ginet et al., 2013)
108 derived from measurements made over an extended period of time by particle detectors
109 and dosimeters on board many satellites in a variety of orbits (see Table 3 in Ginet et
110 al. (2013)), (iii) a Particle ONERA (Office National d'Etudes et de Recherches Aérospatiales/
111 French Aeronautics and Space Research Center)-LANL Electron (POLE) model (Boscher
112 et al., 2003) of energetic electron flux developed using 25 years of LANL data with in-
113 put as the year in the solar cycle, (iv) the extended POLE model known as the new In-
114 ternational Geostationary Electron model (IGE-2006) (Sicard-Piet et al., 2008) created
115 by adding the data from the Japanese spacecraft Data Relay Test Satellite (DRTS), and
116 (v) the electrons model (Roeder et al., 2005) based on Polar HYDRA (Hot Plasma An-

alyzer) data proving the average flux as a function of the position in the Earth's magnetosphere. The models above were not parameterized on geomagnetic conditions and did not capture the magnetic local time (MLT) dependence and variations on time scales of less than a day.

The Kp (Planetary Kennziffer) index, a simple 0-9 index as compared to the more complex variations of solar wind and IMF parameters, has been used to organize keV electron fluxes (e.g., Korth et al., 1999). Using LANL satellites data in the range from 1 eV to 40 keV at GEO, Denton et al. (2015, 2016) developed a model which predicts electron flux values based on energy and local time for given values of the 3-hour Kp-index and $-V_{SW}B_z$ (the electric field of the solar wind, where V_{SW} is the solar wind speed, B_z is the z-component of the IMF), under the assumption that both Kp and the solar wind electric field are correlated with magnetosphere activity, e.g., for Kp: (Freeman, 1974; Thomsen, 2004); for $-V_{SW}B_z$: (Akasofu, 1964; Burton et al., 1975). The Kp version of the model also provides flux values for given values of the daily F10.7 index (solar radio flux at 10.7 cm). However, while the Kp index may correlate well with flux (at least in daily averaged data), it is neither the best predictive parameter, nor what we would consider to be a physical driver of electron flux variations. Kp, as it Earth-based (measured at ground magnetometers), may not represent conditions in the magnetosphere well. It is most likely a proxy measure, representing a combination of both relevant and non-relevant correlated factors, which tells us little about which specific processes drive flux. While the ease of obtaining it might offset this drawback in prediction models, it may be nearly useless in models seeking instead to explain what drives electrons. Its 3 h time cadence may also make it unsuitable even for prediction models, given that electron fluxes fluctuate much more rapidly. The $-V_{SW}B_z$ measure could be an improvement over Kp as it can be obtained at hourly or faster cadence and each is a specific physical parameter rather than a possible conglomeration of generalized response (as the Kp is). However, this measure, alone, only accounts for two possible driving parameters.

Several studies have examined the response of geosynchronous keV electron flux measured at LANL satellites to solar wind parameters. For example, Shi et al. (2009) found electron flux increases due to solar wind dynamic pressure enhancements and Li et al. (2005) and Kellerman and Shprits (2012) concluded that higher solar wind speed results in higher electron fluxes. Hartley et al. (2014) have found an effect of solar wind speed on the 30-600 keV electron density, temperature and energy density from the MAGED (MAGnetospheric Electron Detector) instrument onboard GOES (Geostationary Operational Environmental Satellites) 13-15.

Sillanpää et al. (2017), using 5 years of GOES 13 MAGED electron flux data, fit an empirical model using both solar wind and IMF B_z to predict electron fluxes at 40, 75 and 150 keV energies, after concluding that the other two IMF components and solar wind density, temperature, and pressure were of less importance. This is in line with earlier studies (e.g., Li et al., 2005; Kellerman & Shprits, 2012; Ganushkina et al., 2019). The effects of multiplicative combinations of parameters such as $-V_{SW}B_z$ (Denton et al., 2016) were not studied and it is possible that not a single parameter but the combined effect of multiple driving parameters that result in the observed fast variations of the keV electrons.

Ganushkina et al. (2021) discovered that the AE/AL (Auroral Electrojet/Auroral Lower) indices, together with solar wind speed, provide a better model of the severe environments related to surface charging of satellites by keV electrons measured by LANL (1990-2005) than do IMF B_z , Kp, and solar wind number density. Based on integral electron fluxes, among 400 events of worst-case severe environments (categorized based on four criteria (Matéo-Vélez et al., 2018) of the solar wind and IMF parameters and geomagnetic indices), 100 were in one criterion based on the measured spacecraft potential and 300 in the other 3 criteria based on these electron flux measurements.

169 In recent years, multivariate approaches have been explored to refine and comple-
 170 ment physical and single variable empirical models, and to determine the main driving
 171 parameters of keV electrons. Some techniques used for predictions of mainly MeV ra-
 172 diation belt electrons include linear prediction filters (e.g., Baker et al., 1990; Rigler et
 173 al., 2004; Castillo Tibocho et al., 2021), dynamic linear models (e.g., Osthus et al., 2014),
 174 conditional mutual information (Wing et al., 2022), multiple regression (e.g., Sakaguchi
 175 et al., 2013; Simms et al., 2014, 2016, 2018a, 2018b; Stepanov et al., 2021), neural net-
 176 works (e.g., Koons & Gorney, 1991; Freeman et al., 1998; Ling et al., 2010; Simms & En-
 177 gebretson, 2020), and Nonlinear AutoRegressive Moving Average with eXogenous (NAR-
 178 MAX) inputs (e.g., Balikhin et al., 2011; Boynton et al., 2015; Balikhin et al., 2016; Boyn-
 179 ton et al., 2016).

180 GOES 13-15 40 keV electron flux data were used by Boynton et al. (2019) to de-
 181 velop a model of time series of the electron flux for each of 24 MLTs employing NAR-
 182 MAX methodology. They found that the IMF factor, a combination of IMF B_y and B_z
 183 component, (Balikhin et al., 2010; Boynton et al., 2011) $B_f(t) = B_T(t)\sin^6(\theta(t)/2)$, where
 184 $B_T(t) = \sqrt{B_y(t)^2 + B_z(t)^2}$ and $\theta = \tan^{-1}(B_y(t)/B_z(t))$, controls most of the output
 185 variance. Another important variable was determined to be the solar wind velocity. The
 186 square root of the solar wind pressure and solar wind density were also chosen by the
 187 algorithm but their contributions are small. Boynton et al. (2019) stressed that the time
 188 resolution of the parameters used in the model development influences the importance
 189 of these parameters. For comparison, the earlier study by Boynton et al. (2013), in which
 190 daily averaged 10-100 keV electron fluxes measured at LANL satellites were used, the
 191 role of southward IMF was found to be insignificant.

192 In the present study, we test the influence of several possible drivers of low energy
 193 electron flux (40-150 keV) observed by GOES 13 and GOES 16 satellites: solar wind ve-
 194 locity (V), number density (N), pressure (P), and the electric field (E_y), IMF B_z , and
 195 substorms (as measured by the AE index). We use ARMAX (autoregressive moving ave-
 196 rage transfer function) models both to measure the cumulative effects and to remove
 197 common cycles and trends that may inflate correlations between variables (Simms et al.,
 198 2022). These parameters may act in combination, with influence accumulating over time.
 199 It is also possible that some variables may not influence electron flux directly but indi-
 200 rectly via other parameters. For the latter case, we develop subset models showing pos-
 201 tulated direct and indirect effects.

202 Regression can be a powerful tool for testing which drivers could have a possible
 203 controlling influence on electron flux levels. However, regression on time series data, be-
 204 cause it often violates the assumption of uncorrelated errors, can result in highly inflated
 205 hypothesis test statistics, giving the impression that certain factors may be strong drivers
 206 of flux when they are only cycling or trending in common (Simms et al., 2022). While
 207 this may not be a problem if we are using a regression model to forecast flux, it will in-
 208 validate the hypothesis tests that allow us to determine if solar wind, IMF, and substorm
 209 factors are meaningfully correlated with flux. We may also find that using more of the
 210 information present in the data (i.e., the time behavior) results in more accurate pre-
 211 dictions.

212 There are several approaches to modelling the periodic behavior of a time series.
 213 We will do so with autoregressive (AR) and moving average (MA) terms (Hyndman &
 214 Athanasopoulos, 2018; Pankratz, 1991). When chosen well, these reduce the autocor-
 215 relation in the errors of the model and fully describe the cycling behavior of the series.
 216 With this behavior effectively removed (by the introduction of these terms) the remain-
 217 ing variability in the data can be tested for its response to external factors (the indepen-
 218 dent variables). This last step results in a transfer function model (X), giving the acronym
 219 ARMAX. The ARMA terms therefore partition out the part of the variance due to com-
 220 mon cycling. What we will be left with is the actual relationship between the predictor
 221 and flux.

Further assumptions of regression models, in general, are a linear relationship between response and predictor variables, homoscedasticity (equality of variances in the residual errors), and normally distributed errors. To achieve linearity, we take the logs of the variables (excepting those with both positive and negative values). This not only allows the use of the linear model technique (regression) to describe what may be a non-linear process, it can also normalize the residuals and reduce the heteroscedasticity (non-equality of variances) of the residual error (Neter et al., 1990).

Other studies have used ARMAX modelling to predict higher energy electron fluxes in geostationary orbit, and these provide further information on this approach of describing the underlying cyclical behavior of flux with AR and MA terms (Balikhin et al., 2011, 2016; Boynton et al., 2015, 2016; Simms & Engebretson, 2020; Simms et al., 2022). We note that nonlinearity was introduced into the models of Balikhin et al. (2011) with polynomial terms (square and cubic terms) instead of the logs we use here. Polynomial terms often result in a similar description of nonlinearity as merely taking logs of the variables. Additive polynomial terms may be a better choice if the slope of the relationship cannot be made constant with the log transformation, but there are potential disadvantages. The exponent of a polynomial term is chosen by the researcher, while linearizing the relationship using a log transformation allows the model itself to choose the exponent of the power function. The polynomial approach may also not have the same ability to fix problems of heteroscedasticity and non-normality of the errors. However, although these appear to be significantly different approaches, most relationships in space weather data are such that either approach will give a similar description of the data.

We also note that ARMAX models may sometimes be called ARIMAX models, with the additional I conveying that the data is differenced at some time step n with a $y_t - y_{t-n}$ transformation. However, as we did not find it necessary to difference the present dataset for the full models, ARMAX without the additional I is the more descriptive acronym.

In this study, we extend this previous work by using the ARMAX technique to determine the most influential drivers of lower energy electron flux behavior. While previous studies (e.g., Balikhin et al., 2011) may choose an optimal, parsimonious set of predictors that describe the variance in the dataset (e.g., through the Error Reduction Ratio technique), using least squares regression (as applied to an ARMA model) we are able to show the statistically significant, relative contributions of each parameter rather than reducing the model to only highlight the most essential variables. In other words, we are able to test for the inutility of certain parameters in describing flux, rather than just choosing those parameters that have the strongest correlation. This provides more information on the additive influence of parameters, even if the influence of some is not as strong as others. This results in a deeper understanding of the ensemble effects. We also explore a reduced model consisting of just those parameters we hypothesize are the direct physical drivers of flux: AE (as a measure of electron injections from substorms), pressure, and the solar wind electric field (E_y , or $-VB_z$).

The description of the data is given in Section 2. Section 3 presents the results for drivers for 40-150 keV. The findings are discussed and the conclusions are drawn in Section 4.

2 Data for Defining the keV Electron Drivers

For electron fluxes, we use hourly averaged data from the geostationary GOES-13 satellite. We analyze the measurements from the MAGED instrument consisting of the nine collimated solid state telescopes (e.g., Rowland & Weigel, 2012), each with a 30° full-angle conical field of view. All nine telescopes measured the directional differential electron fluxes in units of $cm^{-2} \cdot s^{-1} \cdot sr^{-1} \cdot keV^{-1}$. We use the fluxes in the first three energy channels where the fluxes are defined at the midpoints of the energy ranges, i.e.,

272 at 40, 75, and 150 keV. We compute one omnidirectionally averaged flux (flight direction-
273 integrated differential electron fluxes) for each of the energies using pitch angles calcu-
274 lated from the onboard magnetometer data following the method presented in Sillanpää
275 et al. (2017) and Ganushkina et al. (2019). The GOES-13 MAGED data of electron fluxes
276 and the data for the pitch angles of each telescope with 5-min averaging are available
277 at <https://www.ngdc.noaa.gov/stp/satellite/goes/dataaccess.html>.

278 The time interval of this study is 10 June 2013 - 6 August 2016. There were min-
279 imal data gaps of only several hours during these time periods. For the time-dependent
280 analyses (ARMAX models) these gaps were filled with linear interpolation between the
281 existing observations.

282 Solar wind parameters (solar wind velocity V , number density N , pressure P , IMF
283 B_z and B_s (including only the southward component of B_z), and the electric field E_y)
284 and magnetic indices (Kp , AE and $SymH$) were obtained from OMNIWeb web (<https://omniweb.gsfc219>
285 [.nasa.gov/form/dx1.html](https://omniweb.gsfc219.nasa.gov/form/dx1.html)) with 1 h resolution with data time-shifted to the bow shock
286 nose. We use an hourly ground ULF wave index (ULF) as a global ULF activity proxy
287 reconstructed from 1-min data from the world-wide array of magnetic stations in the North-
288 ern hemisphere (data available at: <https://doi.org/10.2205/ULF-index>) (Kozyreva et al.,
289 2007; Pilipenko et al., 2017).

290 Analyses based on the least squares regression methodology assume that the re-
291 lationship between predictor and response variables be linear, with the residual errors
292 (that variance that is unexplained by the model) being random, normally distributed,
293 and with equal variance over the range of predicted values. This requirement applies even
294 to such analyses as simple correlation. However, the relationship between flux and pre-
295 dictor parameters is often nonlinear and inspection of the residual errors of these anal-
296 yses performed on non-transformed data shows this nonlinearity, as well as non-normality
297 and an inequality of variances at different levels of the predictors. Fortunately, these prob-
298 lems can usually be fixed by taking the log of at least electron flux, with further improve-
299 ments obtained by taking the log of transformable predictor variables as well. We there-
300 fore take \log_{10} of all variables ≥ 0 . Variables containing zero values which cannot be
301 logged without creating missing values (i.e., Kp) were transformed by adding 1 to all val-
302 ues before the log transformation. B_z and E_y , as they have both positive and negative
303 values, were not logged. Examination of residual plots of the ARMAX models (not shown)
304 showed that this transformation fixed all three problems.

305 Because the dependent variable (electron flux) is log-transformed, this results in
306 nonlinear models between flux and all the variables, a power function relationship for
307 those predictor variables that are also log-transformed, and an exponential function re-
308 lationship for those predictor variables that are not logged.

309 Subsequent to the log transformation, all variables were standardized by subtract-
310 ing that series mean and dividing by its standard deviation. This creates unitless vari-
311 ables (Z-scores) for which regression coefficients (slopes) can be directly compared. Al-
312 though it makes no difference to the outcome of the correlations, we also used the Z-scores
313 for the correlation analysis for consistency. We note, however, that neither the log nor
314 the Z-score transformation reduces either the serial autocorrelation or common cycles
315 seen in these time series datasets. This autocorrelation inflates the simple correlations
316 and must be further dealt with by describing/removing the autocorrelation and common
317 trends and cycles via the introduction of AR and MA terms and/or differencing, as de-
318 scribed below in Section 3.2 (Granger & Newbold, 1974; Simms et al., 2022).

319 ARMAX models were developed in IBM SPSS Statistics (formerly known as the
320 Statistical Package for the Social Sciences), with additional statistical analysis in MAT-
321 LAB.

3 Drivers of 40-150 keV Electrons at Geostationary Orbit

3.1 Cross Correlations of Electron Fluxes with Solar Wind and IMF Parameters and Geomagnetic indices

Simple cross correlations of hourly measured parameters (Figure 1) show values near 0.5 for some parameters, most notably and in keeping with previous studies, V , ULF , and AE (e.g., (Li et al., 2005; Kellerman & Shprits, 2012; Hartley et al., 2014; Simms et al., 2014)). Positive correlations are shown with solid lines, negative with dashed red lines. Correlations are performed between electron flux and individual parameters from each hour (0-48 h) before the flux measurement. At higher electron energies, the AE and ULF correlations are lower, with peak correlations at earlier times. The correlation with V may be somewhat higher, but there is also a tendency for its peak correlation with electron flux to occur earlier at higher energies. The correlation of flux with N is less than that with V , although it does become more prominent at 150 keV, if negative.

B_z and B_s correlations with flux are similar to each other. There appears to be no particular advantage to using the B_s parameter over B_z . (Correlations of B_y with flux at all hours and energies were < 0.05 . This parameter was therefore not studied further.) The negative correlations of B_z and $SymH$ with flux are as expected, as each of these parameters are measured on a negative scale indicating increasing strength at more negative values. While the B_z strength shows less association with flux, $SymH$ and Kp show similar patterns of correlation to each other, likely because both are generalized measures of disturbance at ground magnetometers. These parameters also show an increased correlation at earlier time steps at higher flux energy.

P and E_y are somewhat different from the other variables in that they are mathematical combinations of other measured parameters (V^2 and N , and V and B_z in the cases of P and E_y , respectively), but, at the same time, they may have more physical interpretability. That the P -flux correlation is similar to that of the flux correlation with V or N can be seen where the P correlation drops off in a manner similar to the N correlation, albeit, with some tempering of this decrease as the V correlation rises at the same point in time. The E_y -flux correlation follows the pattern of the B_z -flux correlation nearly exactly.

3.2 Interpretation Problems with Simple Correlations: Poorly Defined Variables, Autocorrelation, and Spurious Correlations

Most of the parameters of Figure 1 show more association with flux in the few hours just prior to a flux measurement at the lower energies, but with maximum correlations at the higher energies occurring further back in time. However, it is difficult to interpret a single peak or even a rise in correlation at a given hour as a physical process that happens at that particular time, given that all these parameters are strongly autocorrelated in time. A variable strongly correlated with itself in previous time steps will show a similar correlation with flux at every one of those time steps, making it impossible to determine the exact time of physical action from simple correlation analysis.

Another difficulty with simple correlation analysis is that correlations between predictor variables may distort the apparent association between a predictor and flux by confounding the true relationship. The well known correlation between V and N , for example, even if it is negative, will result in both predictors showing a correlation with flux, even if only one of them has an actual association. Besides this, any co-cycling variables will show a strong correlation even when there is no association other than a similar response to time. This is a particular difficulty in space weather data where both diurnal cycles and longer cycles are common.

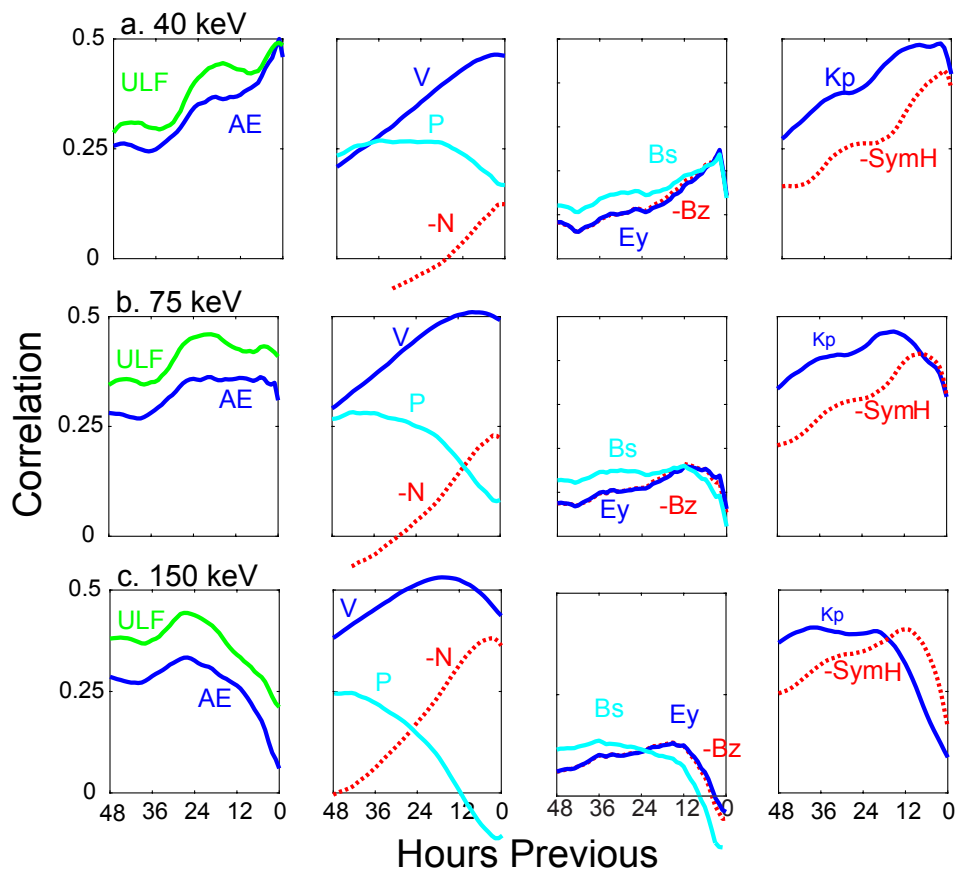


Figure 1. Cross correlations between GOES electron flux and possible drivers (hourly averages) for a. 40 keV, b. 75 keV, c. 150 keV. Solid lines are positive correlations; dashed lines are negative correlations. Note that most correlations are < 0.5 in magnitude.

370 Although we find reasonable correlations of $SymH$ and Kp with flux, to justify in-
 371 cluding these in a model attempting to find the physical drivers of flux, there must be
 372 some basis for thinking there is a physical connection between these particular indices
 373 and electrons. While Kp , derived from midlatitude stations, may be sensitive to vari-
 374 ations at the inner edge of the electron plasma sheet (Thomsen, 2004; Freeman, 1974),
 375 there is no guarantee that this is all or even most of what Kp measures. As the mea-
 376 sure itself is merely the maximum geomagnetic disturbance recorded in a 3 h period, it
 377 may not be specific to that particular area of the magnetosphere, nor temporally fine tuned
 378 enough to be of much use. The discrete nature of the index values would also work to
 379 obscure much of the information it could carry. That there are high correlations between
 380 electron flux and Kp (see Figure 1) is not an argument in favor of its necessary inclu-
 381 sion in a meaningful physical model, but may more likely only indicate that Kp is a proxy
 382 that represents a large number of processes that we would, instead, prefer to know the
 383 effects of individually. In addition, as parameters that are averaged over longer periods
 384 of time tend to show higher statistical correlations without any meaningful increase in
 385 association (Simms et al., 2022), this alone could explain the Kp , at a 3 h cadence, hav-
 386 ing a higher correlation with flux than that of many other parameters. $SymH$ may be
 387 an indirect measure of the free energy available for local wave acceleration of keV elec-
 388 trons up to MeV energies, but is perhaps more representative of inner magnetospheric
 389 plasma pressure, about 12% of which is keV electron pressure (Kumar et al., 2021). $SymH$
 390 may be worth testing as a representation of these processes, but the applicability to elec-
 391 tron flux in the outer radiation belts appears weak. While the AE index can be inter-
 392 preted as a measure of the substorm activity that may result in electron injections, we
 393 do not have the a similarly meaningful physical interpretation of Kp and $SymH$ other
 394 than that they measure the overall level of disturbance in the magnetosphere. But if "dis-
 395 turbance" is a meaningful concept, it is more accurately measured by such parameters
 396 as V , B_z , etc., which also have a physical meaning in the system. In previous work it
 397 has also been found that indices from magnetometers tend to correlate highly with each
 398 other, meaning that it may only be useful, or possible, to include one index in a mul-
 399 tivariate analysis without reaching problematic levels of multicollinearity that make it
 400 impossible to determine which variables are most associated with flux (Simms et al., 2016).
 401 Therefore, we need to use care in deciding which index to use and not include every one
 402 possible. Instead, we should settle on the one that best describes the physical processes
 403 we suspect are occurring.

404 However, these arguments are somewhat moot. If we do include all 3 indices (Kp ,
 405 $SymH$, and AE in a full regression ARMAX model (see below; Table 1), Kp and $SymH$
 406 are not strong candidates, as their influence can be up to an order of magnitude below
 407 that of AE . Although Kp and $SymH$ have high simple correlations with flux, and even
 408 if we were to believe they represented physical drivers, when variables are tested simul-
 409 taneously, these two indices do not perform well. In the subset models, we therefore use
 410 the AE index both because it is representative of substorm activity and because it is a
 411 stronger correlate, at least at 40 keV. In future work, if we planned to create prediction
 412 models only, but not to identify physical drivers, this restriction would not apply and
 413 all three indices could be included (with the caveat that this did not result in overfit-
 414 ting and, therefore, poor predictive ability).

415 Although simple correlations can suggest possible drivers, further work must be done
 416 to elucidate these relationships. Below, in our ARMAX models, we address these issues,
 417 performing multivariate analyses to account for spurious simple correlations due to the
 418 confounding of variables, adding autoregressive (AR) and moving average error (MA)
 419 terms to account for serial autocorrelation and co-cycling of variables, and choosing pre-
 420 dictors that have a reasonable basis for some physical relationship with flux. In regards
 421 to this latter issue, we also choose 4 variables (AE , ULF , P , and E_y) as possible direct
 422 physical drivers of flux (direct effects) and explore their relationship with the other solar
 423 wind and IMF parameters (indirect effects).

424 Additionally, below, we explore whether certain parameters are more correlated during
 425 geomagnetically disturbed periods and at different times of the day. For the former,
 426 we must use a differencing transformation ($y_t - y_{t-1}$) to reduce serial autocorrelation
 427 as, without a complete time series, we are unable to remove this with ARMA terms. To
 428 study varying influences by time of day, we add indicator variables to the ARMAX model
 429 to identify each hour (MLT: magnetic local time).

430 3.3 ARMAX models

431 As noted in the previous section, simple cross correlations of time series variables
 432 may be highly inflated by common cycles and trends often seen in time series data (Granger
 433 & Newbold, 1974). These correlations may, therefore, not say anything useful about the
 434 relationship between variables. In addition, analyzing the effect of each predictor indi-
 435 vidualy gives us no information about the relative importance of each, or the effect of
 436 each when the others are held constant. Multiple regression analysis would assess the
 437 strength of the relationship between each predictor with the effects of the other predic-
 438 tors eliminated. Additionally, as regression gives us the slope of the relationship between
 439 predictor and flux (the coefficients of the regression equation), there will be more infor-
 440 mation about the form of the relationship. We can further improve on a multiple regres-
 441 sion model by introducing terms to specifically describe the cycling, trends, and auto-
 442 correlation that may be present in time series data. These terms may take the form of
 443 an autoregressive component (regressing on previous values of the dependent variable:
 444 an AR term), or a moving average component (regressing on the errors of the model at
 445 preceding time steps: an MA term). A difference term, which subtracts a previous value
 446 from each observation, may also be used to fit an overall trend, but we found this was
 447 not needed for this full set of hourly averaged flux data. For data that cycles “season-
 448 ally” (at a set time period) it may be helpful to also fit seasonal AR and MA terms (Hyndman
 449 & Athanasopoulos, 2018).

450 We fit ARMAX models, using AR and MA terms, along with “seasonal” (daily)
 451 AR and MA terms, to describe the cycling behavior of the dependent variable. We are
 452 then able to test input variables for their possible correlation separate from these com-
 453 mon cycles. The “seasonality” we incorporate is the daily variation in flux seen as the
 454 observing satellite passes between drift shells due to the asymmetric dipole of the Earth’s
 455 magnetic field. Typically, higher energy (MeV) electron flux data collected at geosyn-
 456 chronous orbit shows higher levels on the dayside where the field is compressed and lower
 457 flux levels on the night side where the fields are stretched (e.g., O’Brien & McPherron,
 458 2003; Boynton et al., 2019). For keV electrons, fluxes are highest in the morning hours
 459 and lowest in the evening hours due to their trajectories and losses (e.g., Korth et al.,
 460 1999; Sillanpää et al., 2017).

461 As all variables were standardized by subtracting that series mean and dividing by
 462 its standard deviation, we are able to compare these unitless regression coefficients be-
 463 tween variables. Note that these are not correlation coefficients, but slopes. A 1 unit in-
 464 crease in a predictor variable is thus associated with a certain increase in the dependent
 465 variable. Taking \log_{10} of those variables for which it made sense (i.e., not B_z , for exam-
 466 ple, which has both positive and negative values) effectively creates a non-linear model,
 467 despite how we are using the linear model technique of ARMAX regression.

468 For each electron flux energy (40, 75, and 150 keV), we fit an AR1, MA1,2, sea-
 469 sonal AR1, seasonal MA1 model. More specifically, each regression contained two flux
 470 autoregressive terms (from 1 h previous and 24 h previous) and the moving average of
 471 the errors of the model from 1,2, and 24 h previous as predictors, in addition to the ex-
 472 ogenous AE , Kp , $SymH$, ULF , and solar wind and IMF variables. The 24 h AR and
 473 MA terms represent the “seasonality” terms that model the diurnal fluctuations in flux
 474 due to the movement of the satellite through field lines (in other words, the “seasons”

are days (Table 1). This reduced all terms of the partial autocorrelation function (PACF) to non-statistically significant levels.

3.4 Full ARMAX Model Including All Variables

V , N , IMF B_z , AE , ULF , P , E_y , Kp , and $SymH$ were first entered as numerator (influence) terms at 1 and 2 hour delays, with a denominator (decay) term at 1 hour (Table 1). Influence terms with p-value > 0.10 were dropped from the model. The p-value is the probability that the null hypothesis of no association is true. A p-value < 0.05 is generally considered to be statistically significant, or, put another way, that the null hypothesis of no association has been rejected. (The calculation of the p-value is dependent on the presumed sampling distribution of the test statistic under the null hypothesis, which is itself dependent on the standard error of the estimate. Simply put, dividing the parameter (coefficient) by its standard error gives a t-statistic which can be compared to standard tables giving the probability of that value given the relevant sample sizes. While it can be calculated by hand, it is generally left to the statistical package to do the calculation and table look up (Neter et al., 1990).) Due to this p-value restriction, not all influence and decay terms are retained, however, at least one influence and the decay term are retained for each predictor, even if statistical significance fell above a p-value > 0.10 , in order to describe the relative influence of each term. (The constant term is not significantly different from zero because all variables were standardized and therefore centered around zero. However, we retain it for the small amount of explanatory value it adds to the model.) We report standardized regression coefficients which describe the slope of the relationship between predictor and response variables on a standard (unitless) scale. Due to this standardization we are able to directly compare the influences of each predictor with all the others. (These are slopes, not correlation coefficients, so are not constrained to lie between -1 and 1.)

The R^2 , or coefficient of determination, measures the percent of variation in the data that is explained by the model. (Note that the R^2 is mathematically equivalent to the prediction efficiency used by some other authors when applied to a training dataset.) In simple correlation, the R^2 is equivalent to the square of the correlation coefficient (r^2). The highest simple correlations (e.g. AE and V of Figure 1) around $r = 0.5$ would therefore have an R^2 of 25%, explaining 25% of the variation in the data. Thus, the multiple regression ARMAX models which use both ARMA terms and more than one predictor variable, explain more of the variation than any of the simple correlations. Much of the increase in R^2 is due to the introduction of the ARMA terms, but the ARMAX models do also tell us which independent variables are most important and how they compare in influence with each other. This addition of predictor variables would also allow the ARMAX model to be used for prediction. If there are no exogenous (independent) variables in the model, predictions would quickly revert to the mean value of zero, the constant of the ARMAX equation.

The predictor coefficients can be represented with an empirical prediction equation (Equation 1). For the 40 keV electrons:

$$\begin{aligned}
 Flux_t = & -0.057 + \frac{0.632V_{t-1}}{1 - 0.270V_{t-2}} + \frac{1.087N_{t-1}}{1 - 0.126N_{t-2}} \\
 & + \frac{0.265Bz_{t-1}}{1 - 0.283Bz_{t-2}} + \frac{0.0170Kp_{t-1}}{1 - 0.563Kp_{t-2}} \\
 & + \frac{-0.028SymH_{t-1}}{1 - 0.726SymH_{t-2}} + \frac{0.170AE_{t-1}}{1 - 0.379AE_{t-2}} \\
 & + \frac{0.021ULF_{t-1}}{1 - 0.959ULF_{t-2}} + \frac{-0.992P_{t-1}}{1 - 0.177P_{t-2}}
 \end{aligned}$$

Table 1. ARMAX standardized regression coefficients of the full models (one for each electron energy) including all variables except B_s (*: statistically significant, p-value < 0.05; †: p-value < 0.10; n.s.: not statistically significant, p-value > 0.10)

	40 keV	75 keV	150 keV
Intercept	-0.057n.s	-0.054n.s.	-0.036n.s.
AR1	0.836*	0.845*	0.855*
MA1	0.204*	0.207*	0.069*
MA2	0.302*	0.217*	0.202*
DailyAR1	0.999*	1.000*	1.000*
DailyMA1	0.986*	0.993*	0.994*
V lag 1 h	0.632†	0.888*	-0.196*
Decay	0.270	0.822	-0.147
N lag 1 h	1.087*	1.358*	-0.087*
Decay	0.126	0.811	0.854
Bz lag 1 h	0.265*	0.386*	0.306*
Decay	0.283	0.429	0.673
Kp lag 1 h	0.017n.s.	0.041*	0.023*
Decay	-0.563	0.937	0.967
SymH lag 1 h	-0.028*	-0.004*	0.056*
Decay	0.726	0.975	-0.447
AE lag 1 h	0.170*	0.131*	0.019*
lag 2 h	–	0.050*	0.062*
Decay	0.379*	-0.055	0.551
ULF lag 1 h	0.021*	0.001n.s.	0.003n.s.
Decay	0.959	-0.988	0.984
P lag 1 h	-0.992*	-1.274*	0.035n.s.
Decay	0.177	0.813	0.849
Ey lag 1 h	0.257*	0.352*	0.263*
lag 2 h	-0.131	-0.040*	–
Decay	-0.046	0.414	0.731
R^2	67.4%	69.2%	78.1%

$$\begin{aligned}
& + \frac{0.257Ey_{t-1} - 0.131Ey_{t-2}}{1 - 0.046Ey_{t-2}} \\
& + 0.836 \times \hat{Y}_{t-1} + 0.999 \times \hat{Y}_{t-24} \\
& + 0.204 \times \varepsilon_{t-1} + 0.302 \times \varepsilon_{t-2} + 0.986 \times \varepsilon_{t-24}
\end{aligned} \tag{1}$$

40 keV electron flux at time t is predicted by the other variables at previous times steps ($t - 1$, etc), the model predicted value of flux at $t - 1$ and $t - 24$ ("daily"), and the error between model and observation (ε) at $t - 1$, $t - 2$, and $t - 24$. Each influence term is represented in a numerator, with decay terms in the denominator. For clarity, we do not label the variables that have been logged (flux, V , N , Kp , AE , ULF , and P) in the empirical prediction equation, however, due to this transformation, this is effectively a non linear model in the terms for which we have taken logs. For example, the partial influence coefficient for V of 0.632 would be interpreted as a 1 percent change in the Z score of V resulting in a 0.632 percent change in the Z score of electron flux. However, given the number of differences between our model and that of previous models (including more variables, using Z scores, including decay terms) a direct comparison of these coefficients to other studies using somewhat similar techniques is not particularly meaningful. Instead, it makes more sense to compare which predictor variables are most influential and not the details of exactly how much flux changes in response to a unit change in a predictor.

The influence (numerator) and decay (denominator) terms of Equation 1 give us the tools to calculate the cumulative effects of each input variable. An influence that appears at $t-1$ dissipates at a rate given by the decay term. Thus, although there may only be one hour in which a variable input appears, the exponential decay over time means influence may spread from previous time periods. The influence at a given forward time step from some time step (t) in the past will be that influence $\times (1 - \text{decay factor})^t$. Graphically, this results in a time delay of influence that appears similar to a cross correlation, however, the transfer function gives regression coefficients (i.e., slopes), not correlations. While a correlation can be interpreted as the strength of a relationship between two variables, a regression coefficient can be interpreted as the magnitude of the impact of one variable on another. We use the predictor coefficients of Table 1 to create the cumulative influence bar charts of Figure 2. It should be remembered that these regression coefficients represent the influence of each variable with the others held constant, unlike the simple correlations of Figure 1. Each panel of this figure shows the response of an electron energy (40, 75, and 150 keV) to the influence of each of the 9 exogenous variables when the other 8 predictor variables are held constant. The influence of each begins from the hour previous to the flux measurement. The decay term describes the fall off in influence over time.

These ARMAX models incorporating all 9 possible predictors show little influence of Kp and $SymH$. AE has the highest influence of the geomagnetic indices, but it is weaker than the strong and lasting effects of V , N , and P , particularly at 75 keV. The V , N , and P influences are superficially similar to those seen in the simple cross correlations (Figure 1) but the sign of influence of N and P have switched. B_z and E_y also superficially show the same influence as in the cross correlations, but, again, the sign of influence of B_z is switched.

What are we to make of these losses of influence (particularly Kp and $SymH$) and the changes in sign? It is obvious that simple correlations are highly unreliable as each parameter is highly correlated with all the other parameters of interest, and because any one of them may show a spurious correlation with electron flux due to common cycling behavior.

Second, geomagnetic indices (particularly Kp and $SymH$) do not even appear to influence electron flux when other variables are present. In this full model, Kp and $SymH$

570 have little influence. However, even if they were the most "influential" parameters in these
 571 models, for the reasons mentioned above would we be justified in calling them drivers?
 572 Or are they merely correlated proxies? Is *SymH* a predictor variable at all? Or just an-
 573 other measure of our response variable, the electron flux? These questions can only be
 574 answered from a consideration of what information these indices actually contain. As
 575 we have discussed above, while *Kp* and *SymH* may roughly represent disturbance in the
 576 magnetosphere, we don't know exactly which processes and how much of each process
 577 they might represent. *AE* is a different case. First, *AE* does show more influence than
 578 the other two indices, and second, we know that this index measures substorm activity
 579 which can lead to electron injection. For this latter reason, we will retain *AE* in further
 580 models.

581 Both *P* and *N* act more as a pointed shock to the system with less long term in-
 582 fluence, however, the opposite sign of these two predictors, at similar magnitudes, sug-
 583 gests that there is some degree of multicollinearity occurring between these two. This
 584 is not surprising, as *P*, partially calculated from *N*, is highly correlated with *N* and the
 585 amount of information about the influence of each on flux is almost wholly contained in
 586 the other. Unfortunately, this can result in a pattern of presumed "influence" (as seen
 587 here) that reflects a competition for explanatory power rather than actual opposing ef-
 588 fects on flux, and the inclusion of both in the model is misleading. It is unclear why their
 589 influences appear larger at 75 keV than at 40 or 150 keV, but this could simply be the
 590 result of only a small difference in flux related to the *N* and *P* variables being amplified
 591 by the competition between the two. It is unlikely to represent anything tangible and
 592 only demonstrates that coefficients of highly correlated variables in the same model are
 593 not trustworthy.

594 *B_z* and *E_y* have more modest influences on flux. Despite the high *ULF*-flux cor-
 595 relation seen in the simple correlations, the *ULF* influence on flux is very low. This is
 596 likely due to two factors. First, when other variables are included in the model any proxy
 597 correlation *ULF* may have represented is removed from the *ULF* influence. Second, the
 598 high simple correlation may be simply due to this *ULF* index and satellite-measured flux
 599 both showing a diurnal cycle. When this cycling is removed (via the *AR* and *MA* terms)
 600 the correlation between these variables disappears (Simms et al., 2022). (The occasional
 601 oscillating pattern of influence in several of the variables is the result of a negative de-
 602 cay term found by the regression. It is often unclear whether this has any real physical
 603 meaning.)

604 As these are standardized regression coefficients, we can calculate the impact of a
 605 predictor on flux. For example, as we are using standardized coefficients, a 1 standard
 606 deviation increase in $\log_{10}(AE)$ 1 h previous would result in 0.17 standard deviation in-
 607 crease in $\log_{10}(40keV flux)$, holding all the other predictors constant.

608 3.5 Choice of variables

609 Pressure (*P*) and number density (*N*) are difficult to incorporate into a model si-
 610 multaneously. As pressure is the product of the V^2 and *N*, the strong correlation be-
 611 tween pressure and *N* can lead to unexpected and puzzling behavior. In the models of
 612 Figure 2 and Table 1, there is a strong initial influence of *P*, and an opposing strong in-
 613 fluence of *N* in the same time period. As we know that *P* and *N* are highly correlated
 614 with each other, it is difficult to interpret this as each having a strong, opposing, and,
 615 most importantly, independent influence. It is more likely that these opposing effects are
 616 merely the result of the two terms acting counter to each other in an effort to explain
 617 the same small bit of variation. The same is true of *E_y* with *V* and IMF *B_z*, as *E_y* is the
 618 product of *V* and *B_z*. In fact, it likely makes little sense to draw firm conclusions about
 619 the physical drivers based on this full model. A more plausible model could be achieved
 620 by dropping one of either *P* and *N*, and one of *E_y* and IMF *B_z*. For example, dropping

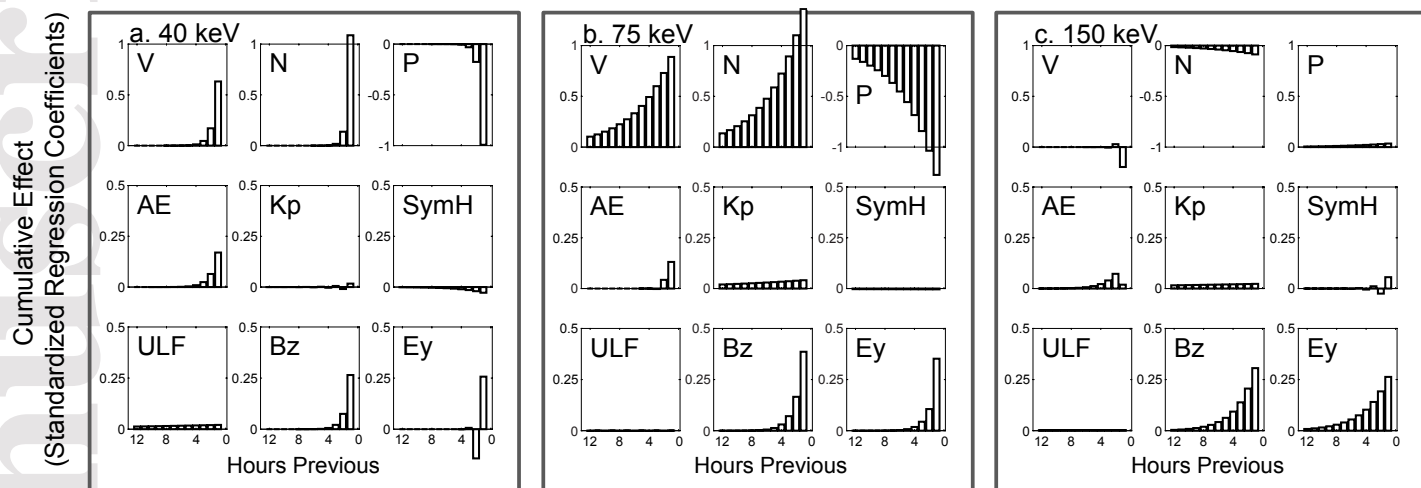


Figure 2. Cumulative effects of all possible drivers of electron flux. For each flux energy, variables are entered simultaneously into an ARMAX regression model as a predictor at a delay of 1 and 2 hours. Only statistically significant time steps are retained, along with a decay factor. Standardized regression coefficients may be compared within each model (a. 40 keV, b. 75 keV, c. 150 keV) to determine the relative influence of each variable on flux. Note that each row has the same scale, but scales vary between rows, in order to compare more effectively between the strongest associations (V , N , and P) and between the indices (AE , Kp , and $SymH$) and other variables with lower influence (ULF , B_z , and E_y).

Table 2. ARMAX standardized regression coefficients of the three reduced models using *AE*, *ULF*, *P*, and *E_y* as predictors (*: statistically significant, p-value < 0.05; n.s.: not statistically significant)

	Log 40 keV flux	Log 75 keV flux	Log 150 keV flux
Constant	-0.090n.s.	-0.093n.s.	-0.056n.s.
AR1	0.825*	0.843*	0.86*
MA1	0.197*	0.195*	0.055*
MA2	0.293*	0.212*	0.201*
Daily AR1	0.998*	0.998*	0.999*
Daily MA1	0.981*	0.987*	0.993*
Log(AE) 1h lag	0.216*	0.130*	0.004n.s.
2h lag	0.154*	0.091*	
Decay 1h	0.882	0.542	0.053
Decay 2 h		0.349	
Log(ULF) 1h lag	0.017*	0.021*	0.03*
Decay 1h	0.965	0.969	0.97
Log(P) 1h lag	-0.025*	-0.039*	-0.055*
Decay 1h	0.717	0.728	0.801
E _y 1h lag	-0.018*	-0.014*	-0.03*
2h lag	—	-0.022	—
Decay 1h	-0.763	-0.381	0.412
<i>R</i> ²	67.10%	68.50%	76.90%

621 the two derived parameters (*E_y* and *P*) would allow us to more accurately see the ef-
622 fects of *V*, *N*, and *B_z*.

623 However, we may be able to do better by separating out just those parameters we
624 believe could be influencing flux directly. These direct parameters would be *AE* (as a
625 measure of substorms which inject electrons), *ULF* (waves in this frequency are thought
626 to drive electrons to higher energies), *E_y* (with the solar wind electric field plausibly hav-
627 ing some influence on electron behavior), and pressure (which could influence flux lev-
628 els through acceleration, through magnetopause shadowing, and by compression of the
629 magnetosphere at the altitude of the satellite, bringing the satellite into higher drift shells
630 with lower electron density). We note that there is little theoretical work to suggest ei-
631 ther *N* or *V* alone drive flux. Their physical action, instead, is thought to derive through
632 pressure. We similarly assume that the physical action of *B_z* is likely through the elec-
633 tric field rather than simply the *B_z* itself. We fit a reduced ARMAX model using only
634 these 4 parameters. The coefficients of this reduced model are presented in Table 2.

635 From the coefficients of this table, we once again calculate the cumulative effects
636 of each variable on flux (Figure 3). At 40 keV (3a), this simpler model of the presumed

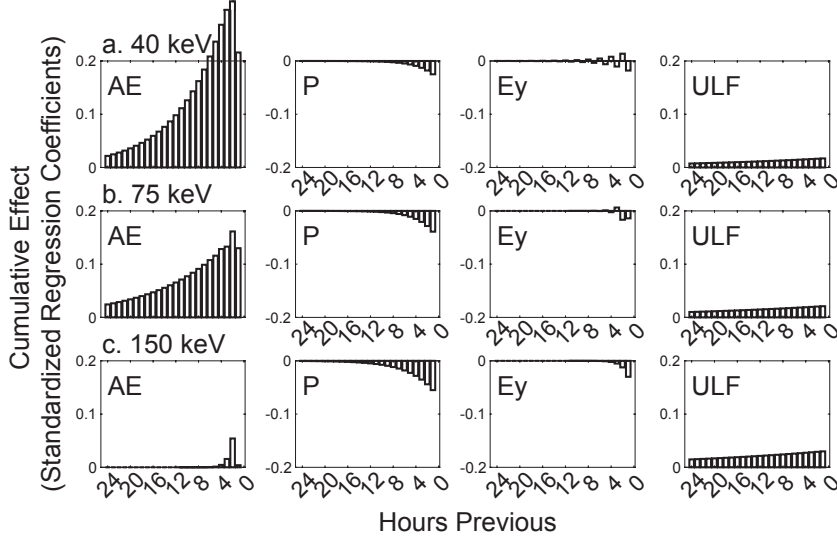


Figure 3. Cumulative effects of the possible direct drivers of electron flux. For each flux energy, AE , P , E_y , and ULF are simultaneously entered into an ARMAX regression model as predictors at 1 and 2 hours, but only significant time steps are retained, along with a decay factor. Standardized partial regression coefficients may be compared within each model to determine the relative influence of each variable on flux: a. 40 keV, b. 75 keV, c. 150 keV.

637 direct effects alone shows a strong effect of AE , peaking at 2 hours before the flux and
 638 with influence over many hours. Pressure, E_y , and ULF , while still statistically signif-
 639 icant effects, are much lower in magnitude. The effect of pressure is negative, presum-
 640 ably as most of its effect is due to the compression of the magnetosphere which positions
 641 the satellite into a less populated drift shell and to magnetopause shadowing. The small
 642 E_y association cycles between positive and negative. A similar pattern is seen for the 75
 643 keV electrons (3b), although the AE influence is slightly lower and the P and ULF ef-
 644 fects somewhat stronger. The 150 keV electrons (3c) show a much lower response to AE ,
 645 and, again, a somewhat stronger response to P and ULF .

646 But what of the strong influence of V we saw in the full model of Figure 2? Although
 647 our direct effects model (of Figure 3) may make more physical sense, we still would like
 648 to understand the correlation of V with flux. We can do this by using the other, indi-
 649 rect parameters to predict our set of more physically interpretable variables, decompos-
 650 ing each correlation into components. In other words, we can use N , V , and IMF B_z to
 651 predict AE , ULF , P , and E_y , which we subsequently use to predict flux.

652 To accomplish this, we presume a causal model (Figure 4) and run a series of re-
 653 regressions to determine the coefficients of the paths. In this figure, we present the stan-
 654 dardized regression coefficients obtained by predicting 40 keV flux from AE , ULF , P ,

655 and E_y . We then predict both AE and ULF using P , E_y , N , V , and IMF B_z from one
 656 hour previous. (These models are not shown explicitly as the input parameter coefficients
 657 are all that we need here, but these are simply the exogenous coefficients from an AR-
 658 MAX model also incorporating AR and MA terms. For this particular model, we use only
 659 a lag 1 h influence term and no decay term to simplify the effects of each input variable.)
 660 Similarly, we show the exogenous variable coefficients for predicting P from N and V ,
 661 and E_y from V and B_z , using N , V , and B_z , but from the same hour as P and E_y . (There
 662 are no paths from V to either ULF or AE because it was not a statistically significant
 663 direct influence on either.) In this figure, green arrows run to and from AE , gold arrows
 664 to and from ULF , and blue arrows to and from P and E_y .

665 These standardized regression coefficients from this series of regression models are
 666 known as path coefficients (Wright, 1934). The path coefficients can be multiplied (through
 667 connecting arrows, or paths), then summed to show the full cumulative effect of each of
 668 the indirect drivers (V , N , and B_z) on the direct drivers (AE , ULF , P , and E_y) and,
 669 subsequently, on flux.

670 The maximum direct effect of each variable is shown by arrows leading directly to
 671 flux. Simple correlations between the exogenous, or indirect, variables (N , V , and B_z)
 672 are shown (in black curved arrows). This decomposition allows the correlation between
 673 a pair of variables to be broken down into direct effects, indirect effects, and spurious
 674 correlation due to associations between the exogenous variables. We are interested in the
 675 direct and indirect effects and will ignore spurious correlations due to the associations
 676 between N , V and B_z . For example, the direct effect of pressure on flux is represented
 677 by the arrow from pressure to flux (-0.04 coefficient). This is rather low, but to this we
 678 can add the indirect effect of pressure: the path from P through AE to flux (coefficients
 679 0.52 and 0.25). This indirect effect of P via its influence on AE (which subsequently in-
 680 fluences flux) is the product of the steps in the path: $0.52 \times 0.25 = 0.13$. The contri-
 681 bution of several indirect paths can be calculated by summing these products (Table 3).
 682 In the first column of this table, we show the direct effect of AE , ULF , P , and E_y on
 683 flux (coefficients on the arrows leading directly to flux of Figure 4). In the second col-
 684 umn we show the results of the calculations for the indirect effects of each variable through
 685 AE , in the third column, these indirect effects through ULF , in the fourth, indirect ef-
 686 fects through P , and in the fifth column, these indirect effects through E_y . (Details of
 687 example calculations are given in the footnote.) The last column is the sum of the first
 688 5 columns, showing the total influence of each variable, both through its direct influence
 689 (if any) and its indirect influence via other parameters.

690 The result of these calculations are that we can now see a clearer picture of which
 691 variables are most influential on flux and through which processes that influence is medi-
 692 ated (given this particular, hypothesized, causal structure). Predictors not postulated
 693 to directly influence flux, such as V , still show an overall moderate degree of influence
 694 when paths connecting it indirectly to flux are considered (mainly, in this case, via P).
 695 However, N , which has a moderate (if negative) simple correlation with 40 keV flux, has
 696 less influence than V when all influences are added. N appears to drive several compet-
 697 ing processes: reducing AE and ULF while simultaneously (through P) increasing flux.
 698 Thus, the lower correlation of N with flux is not an indication that it does not influence
 699 flux, but that it does so through several opposing processes that cancel out each other's
 700 effects in an overall correlation.

701 Certain parameters, such as ULF , which show a strong simple correlation with flux
 702 (Figure 1), are not influential. So why does the simple correlation appear so high in com-
 703 parison? This is due to several factors which we have now accounted for: inflated cor-
 704 relations due to common cycles and trends (accounted for by the AR and MA terms of
 705 the ARMAX regression), correlations with confounding variables (now accounted for by
 706 the use of multivariate regression instead of single correlations), and the possibility that
 707 ULF over the short term (hourly, in this case) has little influence.

Table 3. Calculating the sum of direct and indirect influences on 40 keV flux.

	Direct	via AE	via ULF	Via P	Via Ey	Sum Direct + Indirect Influence
AE	0.25	---	---	---	---	0.25
ULF	0.02	---	---	---	---	0.02
P	-0.04	0.13 ¹	0.018	---	---	0.11
Ey	-0.01	-0.055	-0.005	---	---	-0.070
N	---	-0.12	-0.015	0.12 ²	---	-0.014
V	---	0	0	0.137	-0.0007	-0.024
Bz	---	-0.13	-0.0088	---	0.070	-0.071

¹As an example, the indirect path of P influence through $AE = (\text{effect of P on AE}) \times (\text{effect of AE on flux}) = 0.52 \times 0.25 = 0.13$, using coefficients from the paths in Figure 4.

²The more complicated paths of N through P are summed: $(N \text{ on } P) \times (P \text{ on flux}) + (N \text{ on } P) \times (P \text{ on } AE) \times (AE \text{ on flux}) + (N \text{ on } P) \times (P \text{ on } ULF) \times (ULF \text{ on flux}) = 1.1 \times (-0.04) + 1.1 \times 0.52 \times 0.25 + 1.1 \times 0.88 \times 0.02 = 0.12$.

Table 4. Summed direct and indirect influences on 40, 75, and 150 keV flux.

	a. AE	b. ULF	c. P	d. Ey	e. N	f. V	g. Bz
40 keV	0.25	0.020	0.11	-0.070	-0.014	-0.024	-0.071
75 keV	0.15	0.005	0.021	-0.052	-0.051	-0.049	-0.029
150 keV	-0.001	-0.008	-0.090	-0.023	-0.092	-0.065	0.027

For parameters such as V and N , influence has been diminished by their relegation to indirect driver status in the path analysis. This is a choice made based on the hypothesis that neither is postulated to have the physical ability to directly drive electron flux. If there were reason to believe they did, these could be moved up the hierarchy in the path analysis, allowing them to have more influence in that correlational structure.

We can do these calculations for each of the electron energies, giving the summed influence of each parameter on flux (Table 4). AE appears only as a direct effect, and is thus comparable directly between electron energies, with the strongest effect at 40 keV (0.25) but a lower effect above this range (-0.001 - 0.15). The summed influence of P is generally larger and positive compared to its weak negative direct effect, particularly at 40 keV. The summed E_y effect is similar in magnitude to P . The summed effects of V , N , and B_z are all somewhat equal to each other, with somewhat more effect of V at 40 keV and a higher influence of N at 150 keV. For the most part, these three indirect drivers are negative in influence overall.

3.6 MLT dependence of 40-150 keV electron flux response to AE , ULF , P , and E_y

Electrons at geostationary orbit show different flux levels at different magnetic local times (MLT) (Boynton et al., 2019). With geostationary satellites, which orbit synchronously with MLT, it is unclear whether these are spatial or temporal variations, however, electron injection has been observed in the hours around local midnight (Thomsen et al., 2001; Birn et al., 1997). Using ARMAX models, we investigate not only whether flux differs at varying MLT, but also whether the identified drivers show different influences (i.e., a different coefficient slope) at each MLT. We do not subset the data into MLT bins and analyze them separately, but identify each MLT in the dataset and calculate

a different slope coefficient for each. This is done by creating a set of 23 indicator variables spanning the MLT hours: each is set to 1 for a different, particular MLT and 0 at all other times. The interaction term between each of these indicator variables and each predictor variable (obtained by multiplying each indicator variable by each predictor) gives the slope of the relationship between flux and predictor at each MLT (Neter et al., 1990). By not splitting the dataset by MLT (i.e., by identifying MLT by indicator variables instead), we are able to analyse the dataset as a continual ARMA process. We report these slopes (standardized regression coefficients) for each MLT (Figure 5).

At 40 and 75 keV, AE is the most influential (positive) parameter, but it is most effective over 3-11 MLT (40 keV) and 6-17 MLT (75 keV). Not only is the flux higher at these times (Boynton et al., 2019), but the effect of the strongest driver (AE) is also at its highest level.

The other direct drivers (ULF , P , and E_y) are, as demonstrated above, less influential, but there are MLT differences in their effects. ULF has somewhat more positive effect at 19-0 MLT on the 40 keV electrons. P shows a stronger negative effect over 16-4 MLT, with the most effect being seen at 150 keV. E_y , at 40 and 75 keV, shows a positive effect over 23-8 MLT, with a negative effect over 9-22 MLT. The E_y switch in influence from positive to negative likely accounts for its overall lack of effect in the analyses above that are not broken down by MLT. Although less dramatic, the switch in ULF from positive to slightly negative or near zero also results in an overall lack of influence when MLT is not considered, even though ULF does show a modest positive influence at some times.

3.7 Disturbed vs. quiet response

To produce an ARMAX model, a continuous time series is needed. This means that disturbed and quiet periods must be combined in the same analysis. However, it may be that the flux response to each predictor varies depending on conditions. A simpler multiple regression model could be used to explore the response between quiet and disturbed periods, however, this can result in spurious correlations if variables are cycling together (for example, a diurnal cycle) or show a common trend (Simms et al., 2022). A regression model that accounts for these co-occurring cycles and trends can be produced by differencing the data: subtracting the previous value from each observation ($y_t - y_{t-1}$). This results in regression coefficients that describe the change in flux as predicted by the change in the independent variables, rather than in the original units, but tests of significant influence and comparisons of relative influence can still be made.

To pinpoint those periods when predictors may have differing influence on electron flux due to a change in geomagnetic conditions, we compare disturbed vs. quiet conditions by assembling a subset of "disturbed" hours (a day before and a week following each Dst dip to -100 nT) and a "quiet" set (> 2 weeks after a Dst dip below -30 nT). Within the generalized disturbance periods, we also create a subset ("recovery") with the usually short period of the Dst drop, or storm main phase, removed. The period of time when the Dst is dropping is both short and of less interest to the question of what drives electron flux changes as most of the observable change in this period is due to the compression of the radiation belts below the altitude of the satellite. Following the storm main phase, Dst rises slowly to -30 nT and higher, the recovery and after recovery periods when electron fluxes increase. The rise in electron flux can take up to a week to occur following the main phase, particularly after the strong storms we use in this data subset (Simms et al., 2014). We first perform a multiple regression on the differenced data with AE , ULF , P , and E_y as predictors in order to compare their relative effects via the standardized regression coefficients (Figure 6). We then compare this to the same analyses performed on undifferenced data to show the effect of removing spurious correlations that are the result of common cycles and trends.

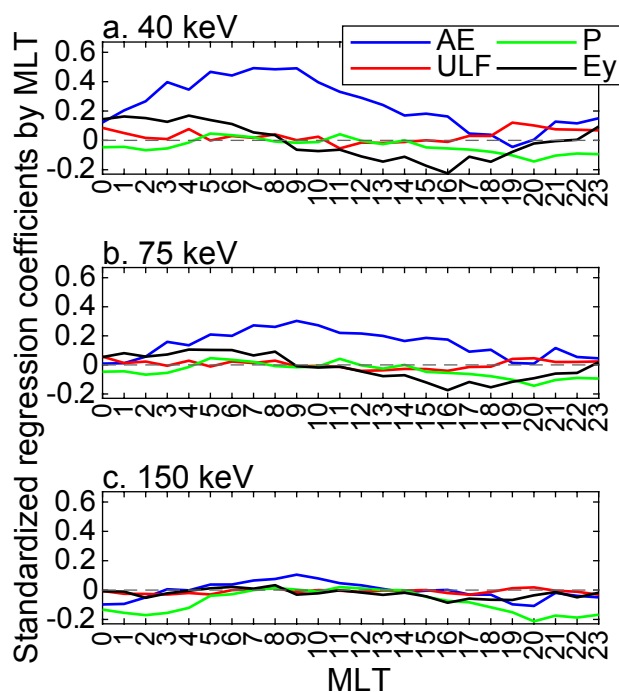


Figure 5. Varying effects of AE , ULF , P , and E_y over magnetic local time. Each variable is entered into an ARMAX regression model as a predictor at 1 h. a. 40 keV, b. 75 keV, c. 150 keV.

784 With differenced data (Figure 6.1), the *AE* effect is consistent over these three pe-
 785 riods (strongest effect on the 40 keV flux, least effect on 150 keV flux). No matter the
 786 geomagnetic conditions, substorms (as measured by *AE*) show a statistically significant
 787 positive influence on flux, with the most effect at the lower electron energies. *P* does not
 788 contribute significantly at most periods or energy levels (the exception being at 150 keV
 789 during disturbed periods). E_y shows a negative effect in the quiet periods but a posi-
 790 tive effect in recovery. *ULF* has little or a negative influence, even when periods are sel-
 791 lected that would be expected to show a strong effect such as recovery following storms.

792 We present an analysis of undifferenced data in this figure (6.2) to show the dan-
 793 ger of correlating variables with common diurnal cycles. In the undifferenced data, we
 794 do find the "expected" strong *ULF* effect (Figure 6.2; note the larger scale compared
 795 to the differenced data), but this is only a demonstration of the spurious nature of this
 796 high correlation. High correlations between *ULF* wave activity and electron flux in hourly
 797 data are likely only describing a common diurnal cycle and say little about physical driv-
 798 ing mechanisms (Simms et al., 2022). Note that it is not so much that the correlation
 799 is "wrong" but that the differencing or ARMA modelling removes the portion of the cor-
 800 relation that is irrelevant to the questions we are interested in. *ULF* waves may be a more
 801 long term driver of flux, with positive influences only appearing after 24 h (Simms et al.,
 802 2021). The other predictors also show stronger effects when not differenced (Figure 6.2),
 803 likely also due to common diurnal cycles in the data.

804 4 Discussion and Conclusions

805 A number of variables show high simple (single variable) correlations with keV elec-
 806 tron flux, but by using an ARMAX analysis, which removes the confounding effect of
 807 diurnal cyclicity and allows assessment of each parameter independently, we show more
 808 definitively that substorms (measured by *AE*) are the most influential process at 40 and
 809 75 keV. This accords with previous work that found substorms to be an important cor-
 810 relate with both keV (Ganushkina et al., 2021) and MeV electrons (Simms et al., 2018a).

811 There are major differences between the single variable correlations and the full
 812 (all variable) ARMAX results. Certain variables lose most of their apparent influence
 813 when all possible drivers are considered at once. Some parameters, for example, *AE*, *Kp*
 814 and *SymH*, may show a decrease in correlation because they all essentially describe the
 815 same geomagnetic perturbations. Although all three geomagnetic indices (*Kp*, *SymH*,
 816 and *AE*) show high simple (single variable) correlations with electron flux, the influences
 817 of *Kp* and *SymH* disappear in a full regression model where other variables are included.
 818 It is likely that these two indices mostly measure generalized disturbance in the mag-
 819 netosphere which is better described using solar wind and IMF variables. However, the
 820 *AE* index, as it is better positioned to measure substorms and subsequent electron in-
 821 jections, is more representative of the physical processes that drive flux.

822 Other variables may appear to lose influence because most of their correlation was
 823 due to sharing a common diurnal cycle with the satellite-observed electron flux data. If
 824 certain of these variables were measured by the same satellite, this would be an obvi-
 825 ous source of error. However, even the *ULF* ground index that we use shows its own di-
 826 urnal cycle and this will inflate the correlation with flux (Simms et al., 2022). Adding
 827 ARMA terms to partition out the variance due to common cycling leaves us with the
 828 portion of the variance that actually describes the relationship between predictor and
 829 flux.

830 Other variables are simply highly correlated with each other (e.g., *N* and *V*), while
 831 others are derived from these same variables (*P* and E_y). This means that single vari-
 832 able analyses, with no correction for cycles and trends, are highly unreliable for pinpoint-
 833 ing the actual correlates of electron flux, and also that variable sets should be chosen to

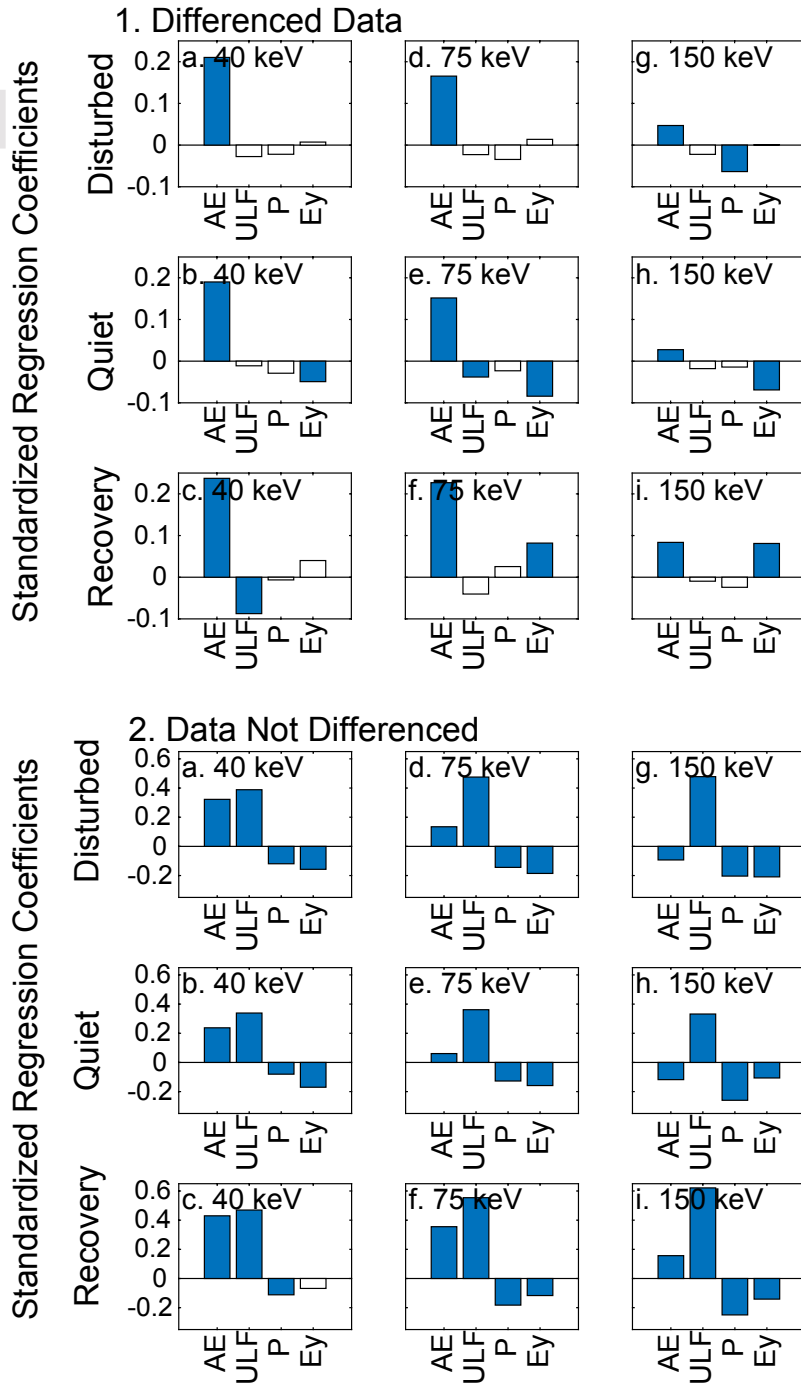


Figure 6. Standardized regression coefficients (AE , ULF , P , and E_y) from multiple regression (not ARMAX) models. 1. All data differenced by subtracting the previous hour's observation: during disturbed periods (a,d,g), quiet periods (b,e,h), and storm recovery periods (c,f,i). 2. The same for undifferenced data. Note the difference in scale between 1. and 2. Significant effects (p-value < 0.05) are shown in blue.

834 minimize these intercorrelations and to maximize the variables of possible direct influ-
835 ence.

836 In the overall ARMAX models, there is a somewhat lesser effect of E_y (calculated
837 as $-V_{SW}B_z$) in contrast to previous single-variable studies (Denton et al., 2016) (but see
838 below, as this may be due to varying influence of this factor over the 24 h period: posi-
839 tive over 23-8 MLT, negative effect over 9-22 MLT). P is more influential at 150 keV,
840 acting to decrease electron flux. The contrast to previous findings, where pressure showed
841 a positive association with flux (Shi et al., 2009), is due to our present study incorpo-
842 rating more predictors at one time. ULF shows little influence on keV electrons in these
843 hourly, full variable models, despite its influence on MeV electrons (Simms et al., 2021,
844 2018a, 2018b) and its strong positive correlation when it is the only predictor and the
845 confounding effects of the diurnal cycle are not removed (Figure 1). This is not to say
846 that ULF waves have no influence, but rather that the single variable correlation mis-
847 characterizes these wave effects as much more dominant than they really are.

848 However, it should be noted that all correlational analysis of this system, whether
849 single variable, multivariable, or correcting for cycles, is observational in nature, not ex-
850 perimental. As treatments cannot be randomly assigned (for example, ULF waves can-
851 not be increased or decreased to explore their effect), the correlations found can only be
852 evidence of an association, not definitive proof of driving. However, despite this, we con-
853 tinue to do the best we can by correcting the issues that we are able to address.

854 As electron flux is log-transformed in our analyses, all the relationships we find here
855 are nonlinear even though they are tested with the linear model method of ARMAX re-
856 gression. As B_z and E_y are not log-transformed, they show an exponential relationship
857 with electron flux. All other predictors, which are log-transformed, are described by a
858 power function relationship. The use of transformations such as the log-transform or poly-
859 nomial terms (Balikhin et al., 2011) are both able to create intrinsically linear regres-
860 sion models from many, but not all, data distributions. However, while both serve to lin-
861 earize the relationship, the log-transform is thought to also help the data to meet other
862 conditions of the linear model framework such as equality and normality of the resid-
863 ual error (Neter et al., 1990).

864 While there are sizable simple correlations of some parameters with electron flux,
865 single variable correlations can misrepresent the actual relationships. If neither common
866 cycles and trends, nor confounding variables are accounted for, simple correlational anal-
867 ysis may show large associations between variables that have no physical relationship.
868 This has been demonstrated before, where removal of common cycles results in either
869 a complete elimination of a correlation between some space weather parameters (e.g.,
870 the commonly observed ULF wave correlation with solar wind velocity or with electron
871 flux (Simms et al., 2022)) or a reduction in correlation (Simms et al., 2021)). An AR-
872 MAX model, used in this study, can account for common cycles in time series data (and
873 trends, if necessary) by the use of AR and MA terms (and differencing, if needed). En-
874 tering several predictor variables into the same analysis then allows each variable's in-
875 fluence to be calculated while the others are held constant.

876 4.1 The Reduced Model: AE , P , E_y , and ULF as predictors

877 However, adding all possible explanatory variables to a model may not correctly
878 identify the most important physical parameters but only those that correlate best, for
879 whatever reason. While a reasonable predictive model may be achieved by using all avail-
880 able variables in a regression or neural network, leaving an algorithm to choose the model
881 with the highest validation correlation, this is unlikely to identify actual drivers in the
882 system. This approach, instead, can lead to several problems: 1. "opposing" variables
883 may appear extremely influential as they compete to explain the same small bit of vari-
884 ation, 2. theoretical considerations of physical influence tend to be ignored in favor of

885 factors that happen to correlate well, 3. coefficient estimates may be biased if extrane-
 886 ous variables are included or if important variables are excluded (Smith, 2018; Whitting-
 887 ham et al., 2006). In the worst case, a model may report that factors that cannot phys-
 888 ically influence the dependent variable are the only factors that have any effect at all.
 889 For this reason, to determine whether a factor has an actual driving influence, care must
 890 be taken to choose only those for which a likely physical effect can be postulated and
 891 not just all that are available. This is why we have chosen to do further analyses on a
 892 set of presumed direct drivers (substorms, ULF waves, pressure, and electric field), as
 893 well as analyses that show the relative correlations of all possible variables.

894 Using the ARMAX method on such a reduced model, we find that the influence
 895 of substorms (AE) on hourly electron flux remains substantial over the 40-75 keV range
 896 at geostationary orbit (approximately L6) although of less importance at 150 keV. This
 897 influence is strongest after midnight into the mid-morning hours MLT, coinciding with
 898 the post midnight to dawn injection of electrons from the magnetotail (Birn et al., 1997;
 899 Thomsen et al., 2001). The AE influence is slightly higher during storm recovery peri-
 900 ods than during either disturbed or quiet periods. Substorms, therefore, are the dom-
 901 inant driver within our postulated "direct driver" set (substorms, ULF waves, solar wind
 902 pressure, and electric field) and presumably show the influx of electrons injected from
 903 the magnetotail.

904 The hourly E_y parameter (electric field of the solar wind) shows little influence when
 905 MLT is ignored. However, introducing MLT into the model results in a positive effect
 906 of E_y over 20-8 MLT, corresponding with the observation that $IMFB_s$ influence is strongest
 907 during this period as well (Dubyagin et al., 2016). There is, however, a mostly negative
 908 effect of E_y at other times of day. These opposing influences cancel each other out in a
 909 model that does not account for variations over MLT. The E_y influence also varies by
 910 geomagnetic conditions, with no influence during disturbed periods, a negative influence
 911 during quiet periods, and a positive influence during recovery after storms. This is likely
 912 a reflection of the magnetospheric electric convective field (which reflects the E_y) break-
 913 ing up during disturbed periods and becoming enhanced during storm recovery.

914 Overall, P shows a moderately negative direct effect on flux. When the analysis
 915 accounts for MLT, this negative influence is strongest over 20-12 MLT.

916 ULF waves, thought to accelerate electrons to higher energies, show lower imme-
 917 diate (hourly) influence than the AE . A strong correlation of ULF waves with high en-
 918 ergy electron flux (> 1.5 MeV) found in previous studies may be a consequence of cor-
 919 relating two variables with a common diurnal cycle, or a reflection of only long term (at
 920 least day long) physical driving (with no short term influence), or both. We find here
 921 that the most significant short term driving of 40-75 keV electrons by ULF appears to
 922 be negative and only during quiet or recovery periods, while there is little short term ef-
 923 fect at 150 keV. The negative short term effect in quiet or recovery periods accords with
 924 previous work on higher energy electrons that shows a negative influence of the ULF in-
 925 dex on the first day, with more positive influences on the next day (Simms et al., 2021),
 926 but is not characteristic of the analyses using all hours. While it is possible that the ULF
 927 index does not effectively capture the immediate, localized, and frequency specific ULF
 928 wave power that would be most responsible for the resonant interaction driving electrons
 929 to these energies (e.g., Claudepierre et al. (2013)), leading to a lower apparent effect, we
 930 note that the ULF index influence is still statistically significant at all 3 energies in anal-
 931 yses using all hours (see Table 2). We have thus captured the importance of ULF waves
 932 as a driver, even if they appear to have less influence than AE once the diurnal cycle is
 933 removed.

934 While all 4 of these factors in the reduced model (AE , P , E_y and ULF) are sta-
 935 tistically significant, the AE has up to 10 times greater influence on the 40-75 keV flux.
 936 This would seem to be the result of electron injection in the lower energy ranges being

937 the major driving factor of increased electron flux. At 150 keV, P and ULF influences
 938 are somewhat stronger than at the lower energies, with their effects being similar to that
 939 of AE . Therefore, electron injection is no longer the most important factor at 150 keV.
 940 Flux, at the higher energy, is more dependent on acceleration due to ULF waves and losses
 941 due to magnetopause shadowing induced by pressure. As noted above, the E_y influence
 942 appears low because it switches in sign from a positive influence post-midnight to a neg-
 943 ative influence post-noon.

944 The amount of variation explained by these reduced (4 factor) models ($R^2 = 67$
 945 - 76 %) is high, but much of this is due to the AR and MA terms that describe the cyc-
 946 cling behavior of flux. In other words, most of what is being explained is the background
 947 rise and fall of flux at the satellite as it orbits the Earth. The explanatory value due to
 948 AE and the other possible drivers pales in comparison, but this is not as discouraging
 949 as it may at first seem. Most of the hourly fluctuation in flux is the rather uninterest-
 950 ing observation that flux varies widely over MLT as the satellite passes through various
 951 field lines. We are more interested in the response of electron flux when this behavior
 952 is eliminated. Once this is removed, we have a clearer picture of which variables are most
 953 influential. The relevant comparison between correlations, then, is not to the single vari-
 954 able, uncorrected correlations of Figure 1 but between the coefficients of the tested possi-
 955 ble drivers of Table 2, and, as previously stated, all of these are statistically significant,
 956 although the AE is the strongest influence at 40-75 keV. (Note that the coefficients of
 957 the ARMAX models are not correlations. They cannot be compared directly to the single
 958 variable correlations of Figure 1.)

959 The response of electron flux to our identified possible direct drivers (AE , ULF ,
 960 P , and E_y) varies only somewhat between disturbed, quiet, and storm recovery periods.
 961 AE is a stronger influence during recovery, for example, than during quiet or disturbed
 962 periods.

963 At 150 keV, there is the least response of hourly averaged flux to the presumed phys-
 964 ical drivers. This may represent the longer time frame of action required from these pro-
 965 cesses to bring electrons to higher energies. Even the cross correlations (Figure 1) show
 966 higher effects from 24-48 hours previous, with ULF and AE showing their least influ-
 967 ence in the 12 h preceding a flux measurement and the E_y influence peaking at 12 h.

968 4.2 Indirect Drivers (N , V , and B_z)

969 In addition to these variables that we label direct, physical drivers of flux, we con-
 970 sider several other parameters as possible indirect drivers (solar wind N and V and IMF
 971 B_z) which show fairly equivalent influences on flux via their effects on the direct drivers.
 972 This supports previous findings concerning these three solar wind and IMF influences
 973 (Sillanpää et al., 2017; Li et al., 2005; Kellerman & Shprits, 2012; Ganushkina et al., 2019;
 974 Hartley et al., 2014). Stepanov et al. (2021) when controlling for other variables, also
 975 found solar wind velocity and a magnetospheric convection variable (the dayside merg-
 976 ing electric field, similar to the E_y we use) to be the strongest correlates of keV flux near
 977 the plasmashet midplane. (A similar multiplicative variable, the IMF factor (Balikhin
 978 et al., 2010; Boynton et al., 2011), and solar wind velocity appear to control hourly aver-
 979 aged 40 keV electrons. However, these last studies did not include a test of AE influ-
 980 ence for comparison.)

981 We note again that we are not trying to predict flux. We are trying to understand
 982 what drives it. We do not test N , V , and B_z for their direct effect on flux in the reduced
 983 model for the simple reason that we have not hypothesized a direct physical connection
 984 between these variables and flux. There is little theory that would suggest this. There
 985 is theoretical work suggesting direct influences of pressure (the combination of N and
 986 V^2), AE (through substorm injection of electrons), and ULF waves (either accelerating
 987 electrons to these energies or causing electron loss). Therefore, we test those particular

988 hypotheses with an ARMAX regression model (the upper part of Figure 4 and the de-
 989 scription in Section 4.1). Although V or N may show a strong single variable correla-
 990 tion with electron flux, this is either via their role in pressure, or via their influence on
 991 ULF waves. These second hypotheses about the indirect V or N influence on flux are
 992 tested in the lower part of Figure 4. By only including hypothesized direct drivers in the
 993 top part of Figure 4, we are better able to test these particular hypotheses. If we include
 994 N and V , as in the full regression model, then we are no longer testing hypotheses about
 995 direct drivers and, in fact, are making those particular hypothesis tests impossible be-
 996 cause of the interference between these variables.

997 We are able to compare effects of the other correlates by summing their indirect
 998 influence through the presumed physical drivers. We are able to calculate that at 40 keV,
 999 P shows a summed influence (both direct and indirect) nearly half that of the most in-
 1000 influential parameter, AE , with E_y having about a fourth the influence of AE . Of the pos-
 1001 tulated indirect drivers, N , B_z , and V show nearly equal effects. The N and V influences
 1002 are negative, while the B_z influence switches sign above 75 keV.

1003 4.3 The Problem of Prediction vs. Driver Identification

1004 If the purpose of a model is accurate prediction, then a simple validation correla-
 1005 tion of observation with prediction on a withheld test set is the statistic of interest. In
 1006 that case, predictor variables can be chosen simply on the basis of availability and abil-
 1007 ity to correlate well with the response. Alternatively, the ARMAX-regression models we
 1008 present here address the question of what parameters drive flux changes. We use hypoth-
 1009 esis testing within the ARMAX-regression framework to determine whether certain param-
 1010 eters show an association with electron flux. As our questions concern the science
 1011 of the system (i.e., which variables are drivers), we consider, first, which variables most
 1012 justifiably have a physical association with flux and which are only highly correlated be-
 1013 cause they are proxies. Of particular concern is the removal of the diurnal cycle due to
 1014 satellite orbit. This factor alone may increase apparent correlations tremendously with-
 1015 out having any bearing on the physical driving relationships.

1016 A model such as this, developed for determining the actual relationships, statisti-
 1017 cally tests the slope of association with flux for each identified variable, with less con-
 1018 cern attached to either a validation correlation or the overall R^2 (proportion of varia-
 1019 tion explained). That these more focused hypothesis tests appear to explain less than
 1020 the unspecific correlations only reflects the removal of spurious correlations that lead to
 1021 an incorrect understanding of the system.

1022 Acknowledgments

1023 We thank the anonymous reviewers whose comments improved this manuscript. The work
 1024 at the University of Michigan was partly funded by National Aeronautics and Space Ad-
 1025 ministration grants NNX17AI48G, 80NSSC20K0353, and National Science Foundation
 1026 grant 1663770. The contributions by S. Dubyagin, M. van de Kamp and N. Ganushk-
 1027 ina were also partly supported by the Academy of Finland (grant 339329).

1028 The GOES-13 MAGED data and GOES Magnetometer 1 data used in the present
 1029 study are available at <https://www.ngdc.noaa.gov/stp/satellite/goes/dataaccess.html>.
 1030 Solar wind parameters and magnetic indices were obtained from OMNIWeb (<https://omniweb.gsfc>
 1031 [219 .nasa.gov/form/dx1.html](https://omniweb.gsfc.nasa.gov/form/dx1.html)).

1032 References

1033 Akasofu, S.-I. (1964). A source of the energy for geomagnetic storms and auroras.
 1034 *Planetary Space Science*, 12, 801.

- 1035 Baker, D. N., Hoxie, V., Zhao, H., Jaynes, A. N., Kanekal, S., Li, X., & Elkington,
1036 S. (2019). Multiyear measurements of radiation belt electrons: Acceleration,
1037 transport, and loss. *Journal of Geophysical Research: Space Physics*, *124*,
1038 25882602. doi: <https://doi.org/10.1029/2018JA026259>
- 1039 Baker, D. N., McPherron, R. L., Cayton, T. E., & Klebesadel, R. W. (1990). Lin-
1040 ear prediction filter analysis of relativistic electron properties at 6.6 re. *Journal*
1041 *of Geophysical Research: Space Physics*, *95*(A9), 15133-15140. doi: [https://doi](https://doi.org/10.1029/JA095iA09p15133)
1042 [.org/10.1029/JA095iA09p15133](https://doi.org/10.1029/JA095iA09p15133)
- 1043 Balikhin, M. A., Boynton, R. J., Billings, S. A., Gedalin, M., Ganushkina, N., Coca,
1044 D., & Wei, H. (2010). Data based quest for solar wind-magnetosphere coupling
1045 function. *Geophysical Research Letters*, *37*(24). doi: [https://doi.org/10.1029/](https://doi.org/10.1029/2010GL045733)
1046 [2010GL045733](https://doi.org/10.1029/2010GL045733)
- 1047 Balikhin, M. A., Boynton, R. J., Walker, S. N., Borovsky, J. E., Billings, S. A., &
1048 Wei, H. L. (2011). Using the narmax approach to model the evolution of en-
1049 ergetic electrons fluxes at geostationary orbit. *Geophysical Research Letters*,
1050 *38*(18). doi: <https://doi.org/10.1029/2011GL048980>
- 1051 Balikhin, M. A., Rodriguez, J., R.J., B., Walker, S., Aryan, H., Sibeck, D., &
1052 Billings, S. (2016). Comparative analysis of noaa refm and snb3geo tools
1053 for the forecast of the fluxes of high-energy electrons at geo. *Space Weather*,
1054 *14*, 22-31. doi: [doi:10.1002/2015SW001303](https://doi.org/10.1002/2015SW001303)
- 1055 Birn, J., Thomsen, M. F., Borovsky, J. E., Reeves, G. D., McComas, D. J., & Be-
1056 lian, R. D. (1997). Characteristic plasma properties of dispersionless substorm
1057 injections at geosynchronous orbit. *Journal of Geophysical Research*, *102*,
1058 2309. doi: [10.1029/96JA02870](https://doi.org/10.1029/96JA02870)
- 1059 Blake, J. B., Baker, D. N., Turner, N., Ogilvie, K. W., & Lepping, R. P. (1997).
1060 Correlation of changes in the outer-zone relativistic-electron population with
1061 upstream solar wind and magnetic field measurements. *Geophysical Research*
1062 *Letters*, *24*(8), 927-929. doi: <https://doi.org/10.1029/97GL00859>
- 1063 Boscher, D., Bourdarie, S., Friedel, R., & Belian, R. (2003). Model for the geo-
1064 stationery electron environment: Pole. *IEEE Transactions on Nuclear Science*,
1065 *50*(6), 2278-2283. doi: [10.1109/TNS.2003.821609](https://doi.org/10.1109/TNS.2003.821609)
- 1066 Boynton, R. J., Amariutei, O. A., Shprits, Y. Y., & Balikhin, M. A. (2019).
1067 The system science development of local time-dependent 40-keV electron
1068 flux models for geostationary orbit. *Space Weather*, *17*(6), 894-906. doi:
1069 <https://doi.org/10.1029/2018SW002128>
- 1070 Boynton, R. J., Balikhin, M. A., & Billings, S. A. (2015). Online narmax model for
1071 electron fluxes at geo. *Annales Geophysicae*, *33*, 405-411. doi: [doi:10.5194/](https://doi.org/10.5194/angeo-33-405-2015)
1072 [angeo-33-405-2015](https://doi.org/10.5194/angeo-33-405-2015)
- 1073 Boynton, R. J., Balikhin, M. A., Billings, S. A., Reeves, G. D., Ganushkina, N.,
1074 Gedalin, M., . . . Walker, S. N. (2013). The analysis of electron fluxes at
1075 geosynchronous orbit employing a narmax approach. *Journal of Geophysical*
1076 *Research: Space Physics*, *118*(4), 1500-1513. doi: [https://doi.org/10.1002/](https://doi.org/10.1002/jgra.50192)
1077 [jgra.50192](https://doi.org/10.1002/jgra.50192)
- 1078 Boynton, R. J., Balikhin, M. A., Billings, S. A., Wei, H. L., & Ganushkina, N.
1079 (2011). Using the narmax ols-err algorithm to obtain the most influential
1080 coupling functions that affect the evolution of the magnetosphere. *Journal of*
1081 *Geophysical Research: Space Physics*, *116*(A5). doi: [https://doi.org/10.1029/](https://doi.org/10.1029/2010JA015505)
1082 [2010JA015505](https://doi.org/10.1029/2010JA015505)
- 1083 Boynton, R. J., Balikhin, M. A., Sibeck, D. G., Walker, S. N., Billings, S. A., &
1084 Ganushkina, N. (2016). Electron flux models for different energies at geosta-
1085 tionary orbit. *Space Weather*, *14*, 846-860. doi: [doi:10.1002/2016SW001506](https://doi.org/10.1002/2016SW001506)
- 1086 Burton, R. K., McPherron, R. L., & Russell, C. T. (1975). An empirical relationship
1087 between interplanetary conditions and dst. *Journal of Geophysical Research*,
1088 *80*, 42044214. doi: [10.1029/JA080i031p04204](https://doi.org/10.1029/JA080i031p04204)
- 1089 Castillo Tibocho, A. M., de Wiljes, J., Shprits, Y. Y., & Aseev, N. A. (2021). Re-

- 1090 constructing the dynamics of the outer electron radiation belt by means of the
 1091 standard and ensemble kalman filter with the verb-3d code. *Space Weather*,
 1092 *19*(10), e2020SW002672. doi: <https://doi.org/10.1029/2020SW002672>
- 1093 Chen, M. W., Lemon, C. L., Orlova, K., Shprits, Y., Hecht, J., & Walterscheid,
 1094 R. L. (2015). Comparison of simulated and observed trapped and precipitating
 1095 electron fluxes during a magnetic storm. *Geophysical Research Letters*, *42*(20),
 1096 8302-8311. doi: <https://doi.org/10.1002/2015GL065737>
- 1097 Choi, H. S., Lee, J., Cho, K. S., Kwak, Y. S., Cho, I. H., Park, Y. D., . . . Lee, D. K.
 1098 (2011). Analysis of GEO spacecraft anomalies: Space weather relationships.
 1099 *Sp. Weather*, *9*(5), 1–12. doi: 10.1029/2010SW000597
- 1100 Claudepierre, S. G., Mann, I. R., Takahashi, K., Fennell, J. F., Hudson, M. K.,
 1101 Blake, J. B., . . . Wygant, J. R. (2013). Van allen probes observation of
 1102 localized drift resonance between poloidal mode ultra-low frequency waves
 1103 and 60 keV electrons. *Geophysical Research Letters*, *40*, 44914497. doi:
 1104 10.1002/grl.50901
- 1105 Denton, M. H., Henderson, M. G., Jordanova, V. K., Thomsen, M., Borovsky, J. E.,
 1106 Woodroffe, J., . . . Pitchford, D. (2016). An improved empirical model of
 1107 electron and ion fluxes at geosynchronous orbit based on upstream solar wind
 1108 conditions. *Space Weather*, *14*(7), 511-523. doi: 10.1002/2016SW001409
- 1109 Denton, M. H., Thomsen, M., Jordanova, V. K., Henderson, M. G., Borovsky, J. E.,
 1110 Denton, J. S., . . . Hartley, D. P. (2015). An empirical model of electron and
 1111 ion fluxes derived from observations at geosynchronous orbit. *Space Weather*,
 1112 *13*(4), 233-249. doi: 10.1002/2015SW001168
- 1113 Dubyagin, S., Ganushkina, N. Y., Sillanp, I., & Runov, A. (2016). Solar wind-driven
 1114 variations of electron plasma sheet densities and temperatures beyond geo-
 1115 stationary orbit during storm times. *Journal of Geophysical Research: Space*
 1116 *Physics*, *121*, 83438360. doi: 10.1002/2016JA022947
- 1117 Fok, M.-C., Buzulukova, N. Y., Chen, S.-H., Glocer, A., Nagai, T., Valek, P., &
 1118 Perez, J. D. (2014). The comprehensive inner magnetosphere-ionosphere
 1119 model. *Journal of Geophysical Research: Space Physics*, *119*(9), 7522-7540.
 1120 doi: 10.1002/2014JA020239
- 1121 Freeman, J. W. (1974). Kp dependence of plasma sheet boundary. *Journal of Geo-*
 1122 *physical Research*, *79*, 4315.
- 1123 Freeman, J. W., O'Brien, T. P., Chan, A. A., & Wolf, R. A. (1998). Energetic
 1124 electrons at geostationary orbit during the november 3-4, 1993 storm: Spa-
 1125 tial/temporal morphology, characterization by a power law spectrum and,
 1126 representation by an artificial neural network. *Journal of Geophysical Re-*
 1127 *search: Space Physics*, *103*(A11), 26251-26260. doi: [https://doi.org/10.1029/](https://doi.org/10.1029/97JA03268)
 1128 [97JA03268](https://doi.org/10.1029/97JA03268)
- 1129 Ganushkina, N. Y., Liemohn, M. W., Amariutei, O. A., & Pitchford, D. (2014).
 1130 Low-energy electrons (5-50 keV) in the inner magnetosphere. *Journal*
 1131 *of Geophysical Research: Space Physics*, *119*(1), 246-259. doi: 10.1002/
 1132 2013JA019304
- 1133 Ganushkina, N. Y., Sillanp, I., Welling, D., Haiducek, J., Liemohn, M., Dubyagin,
 1134 S., & Rodriguez, J. V. (2019). Validation of inner magnetosphere particle
 1135 transport and acceleration model (imptam) with long-term goes maged mea-
 1136 surements of keV electron fluxes at geostationary orbit. *Space Weather*, *17*(5),
 1137 687-708. doi: <https://doi.org/10.1029/2018SW002028>
- 1138 Ganushkina, N. Y., Swiger, B., Dubyagin, S., Matéo-Vélez, J.-C., Liemohn, M. W.,
 1139 Sicard, A., & Payan, D. (2021). Worst-case severe environments for sur-
 1140 face charging observed at lanl satellites as dependent on solar wind and
 1141 geomagnetic conditions. *Space Weather*, *19*(9), e2021SW002732. doi:
 1142 <https://doi.org/10.1029/2021SW002732>
- 1143 Ginet, G. P., O'Brien, T. P., Huston, S. L., Johnston, W. R., Guild, T. B., Friedel,
 1144 R., . . . Su, Y.-J. (2013). Ae9, ap9 and spm: New models for specifying the

- 1145 trapped energetic particle and space plasma environment. *Space Science Re-*
 1146 *views*, 179, 579615. doi: 10.1007/s11214-013-9964-y
- 1147 Granger, C., & Newbold, P. (1974). Spurious regressions in econometrics. *Journal of*
 1148 *Econometrics*, 2(2), 111-120. doi: [https://doi.org/10.1016/0304-4076\(74\)90034-](https://doi.org/10.1016/0304-4076(74)90034-7)
 1149 [7](https://doi.org/10.1016/0304-4076(74)90034-7)
- 1150 Harel, M., Wolf, R., Spiro, R., Reiff, P., Chen, C.-K., Burke, W., ... Smiddy, M.
 1151 (1981). Quantitative simulation of a magnetospheric substorm 2, comparison
 1152 with observations. *Journal of Geophysical Research*, 86, 22422260.
- 1153 Hartley, D. P., Denton, M. H., & Rodriguez, J. V. (2014). Electron number density,
 1154 temperature, and energy density at geo and links to the solar wind: A simple
 1155 predictive capability. *Journal of Geophysical Research: Space Physics*, 119(6),
 1156 4556-4571. doi: <https://doi.org/10.1002/2014JA019779>
- 1157 Hyndman, R., & Athanasopoulos, G. (2018). *Forecasting: Principles and practice*.
 1158 Heathmont, Victoria, Australia: OTexts.
- 1159 Jordanova, V. K., Tu, W., Chen, Y., Morley, S. K., Panaitescu, A.-D., Reeves,
 1160 G. D., & Kletzing, C. A. (2016). Ram-scb simulations of electron trans-
 1161 port and plasma wave scattering during the october 2012 double-dip storm.
 1162 *Journal of Geophysical Research: Space Physics*, 121(9), 8712-8727. doi:
 1163 <https://doi.org/10.1002/2016JA022470>
- 1164 Kellerman, A. C., & Shprits, Y. Y. (2012). On the influence of solar wind conditions
 1165 on the outer-electron radiation belt. *Journal of Geophysical Research: Space*
 1166 *Physics*, 117(A5). doi: <https://doi.org/10.1029/2011JA017253>
- 1167 Koons, H. C., & Gorney, D. J. (1991). A neural network model of the relativistic
 1168 electron flux at geosynchronous orbit. *Journal of Geophysical Research: Space*
 1169 *Physics*, 96(A4), 5549-5556. doi: <https://doi.org/10.1029/90JA02380>
- 1170 Koons, H. C., Mazur, J. E., Selesnick, R. S., Blake, J. B., Fennell, J. F., Roeder,
 1171 J. L., & Anderson, P. C. (2000). *The impact of the space environment on space*
 1172 *systems* (Vol. AFRL-VS-TR-20001578).
- 1173 Korth, H., Thomsen, M., Borovsky, J. E., & McComas, D. J. (1999). Plasma
 1174 sheet access to geosynchronous orbit. *Journal of Geophysical Research: Space*
 1175 *Physics*, 104(A11), 25047-25061. doi: <https://doi.org/10.1029/1999JA900292>
- 1176 Kozyreva, O., Pilipenko, V., Engebretson, M., Yumoto, K., Watermann, J., & Ro-
 1177 manova, N. (2007). In search of a new ulf wave index: Comparison of pc5
 1178 power with dynamics of geostationary relativistic electrons. *Planetary Space*
 1179 *Sciences*, 55, 755. doi: [doi:10.1016/j.pss.2006.03.013](https://doi.org/10.1016/j.pss.2006.03.013)
- 1180 Kumar, S., Miyoshi, Y., Jordanova, V. K., Engel, M., Asamura, K., Yokota, S., &
 1181 et al. (2021). Contribution of electron pressure to ring current and ground
 1182 magnetic depression using ram-scb simulations and arase observations during
 1183 78 november 2017 magnetic storm. *Journal of Geophysical Research:Space*
 1184 *Physics*, 126, e2021JA029109. doi: <https://doi.org/10.1029/2021JA029109>
- 1185 Lam, H.-L., Boteler, D. H., Burlton, B., & Evans, J. (2012). Anik-e1 and e2 satel-
 1186 lite failures of january 1994 revisited. *Space Weather*, 10(10). doi: [10.1029/](https://doi.org/10.1029/2012SW000811)
 1187 [2012SW000811](https://doi.org/10.1029/2012SW000811)
- 1188 Li, X., Baker, D. N., Temerin, M., Reeves, G., Friedel, R., & Shen, C. (2005). En-
 1189 ergetic electrons, 50 keV to 6 MeV, at geosynchronous orbit: Their responses
 1190 to solar wind variations. *Space Weather*, 3(4). doi: [https://doi.org/10.1029/](https://doi.org/10.1029/2004SW000105)
 1191 [2004SW000105](https://doi.org/10.1029/2004SW000105)
- 1192 Li, X., Temerin, M., Baker, D. N., Reeves, G. D., & Larson, D. (2001). Quantita-
 1193 tive prediction of radiation belt electrons at geostationary orbit based on solar
 1194 wind measurements. *Geophysical Research Letters*, 28(9), 1887-1890. doi:
 1195 <https://doi.org/10.1029/2000GL012681>
- 1196 Ling, A. G., Ginet, G. P., Hilmer, R. V., & Perry, K. L. (2010). A neural net-
 1197 workbased geosynchronous relativistic electron flux forecasting model. *Space*
 1198 *Weather*, 8(9). doi: <https://doi.org/10.1029/2010SW000576>
- 1199 Loto'aniu, T. M., Singer, H. J., Rodriguez, J. V., Green, J., Denig, W., Biesecker,

- 1200 D., & Angelopoulos, V. (2015). Space weather conditions during the
1201 galaxy 15 spacecraft anomaly. *Space Weather*, *13*(8), 484-502. doi:
1202 10.1002/2015SW001239
- 1203 Lyatsky, W., & Khazanov, G. V. (2008). Effect of solar wind density on relativistic
1204 electrons at geosynchronous orbit. *Geophysical Research Letters*, *35*(3). doi:
1205 https://doi.org/10.1029/2007GL032524
- 1206 Matéo-Vélez, J.-C., Sicard, A., Payan, D., Ganushkina, N., Meredith, N. P., & Sil-
1207 lanpää, I. (2018). Spacecraft surface charging induced by severe environments
1208 at geosynchronous orbit. *Space Weather*, *16*. doi: 10.1002/2017SW001689
- 1209 Neter, J., Kutner, M. H., & Wassermann, W. (1990). *Applied linear statistical mod-*
1210 *els, 3rd ed.* Homewood, Illinois, USA: Irwin.
- 1211 O'Brien, T. P., & McPherron, R. L. (2003). An empirical dynamic equation for
1212 energetic electrons at geosynchronous orbit. *Journal of Geophysical Research*,
1213 *108*(A3), 1137. doi: 10.1029/2002JA009324
- 1214 Osthus, D., Caragea, P. C., Higdon, D., Morley, S. K., Reeves, G. D., & Weaver,
1215 B. P. (2014). Dynamic linear models for forecasting of radiation belt electrons
1216 and limitations on physical interpretation of predictive models. *Space Weather*,
1217 *12*(6), 426-446. doi: https://doi.org/10.1002/2014SW001057
- 1218 Pankratz, A. (1991). *Forecasting with dynamic regression models.* New York, USA:
1219 John Wiley and Sons, Inc.
- 1220 Paulikas, G., & Blake, J. (1979). Effects of the solar wind on magnetospheric
1221 dynamics: Energetic electrons at the synchronous orbit. In *Quantitative mod-*
1222 *eling of magnetospheric processes* (p. 180-202). American Geophysical Union
1223 (AGU). doi: https://doi.org/10.1029/GM021p0180
- 1224 Pilipenko, V. A., Kozyreva, O., Engebretson, M., & Soloviev, A. (2017). Ulf wave
1225 power index for space weather and geophysical applications: A review. *Russian*
1226 *Journal of Earth Sciences*, *17*(ES1004). doi: doi:10.2205/2017ES000597
- 1227 Pulkkinen, T. I., Dimmock, A. P., Lakka, A., Osmane, A., Kilpua, E., Myllys, M.,
1228 ... Viljanen, A. (2016). Magnetosheath control of solar windmagnetosphere
1229 coupling efficiency. *Journal of Geophysical Research: Space Physics*, *121*,
1230 87288739. doi: 10.1002/2016JA023011
- 1231 Reeves, G. D., Morley, S. K., Friedel, R. H. W., Henderson, M. G., Cayton, T. E.,
1232 Cunningham, G., ... Thomsen, D. (2011). On the relationship between
1233 relativistic electron flux and solar wind velocity: Paulikas and blake re-
1234 visited. *Journal of Geophysical Research: Space Physics*, *116*(A2). doi:
1235 https://doi.org/10.1029/2010JA015735
- 1236 Rigler, E. J., Baker, D. N., Weigel, R. S., Vassiliadis, D., & Klimas, A. J. (2004).
1237 Adaptive linear prediction of radiation belt electrons using the kalman filter.
1238 *Space Weather*, *2*(3). doi: https://doi.org/10.1029/2003SW000036
- 1239 Roeder, J. L., Chen, M. W., Fennell, J. F., & Friedel, R. (2005). Empirical models of
1240 the low-energy plasma in the inner magnetosphere. *Space Weather*, *3*(12). doi:
1241 https://doi.org/10.1029/2005SW000161
- 1242 Rowland, W., & Weigel, R. S. (2012). Intracalibration of particle detectors on a
1243 three-axis stabilized geostationary platform. *Space Weather*, *10*(11). doi: 10
1244 .1029/2012SW000816
- 1245 Sakaguchi, K., Miyoshi, Y., Saito, S., Nagatsuma, T., Seki, K., & Murata, K. T.
1246 (2013). Relativistic electron flux forecast at geostationary orbit using kalman
1247 filter based on multivariate autoregressive model. *Space Weather*, *11*(2), 79-89.
1248 doi: https://doi.org/10.1002/swe.20020
- 1249 Shi, Y., Zesta, E., & Lyons, L. R. (2009). Features of energetic particle ra-
1250 dial profiles inferred from geosynchronous responses to solar wind dy-
1251 namic pressure enhancements. *Annales Geophysicae*, *27*(2), 851-859. doi:
1252 10.5194/angeo-27-851-2009
- 1253 Sicard-Piet, A., Bourdarie, S., Boscher, D., Friedel, R. H. W., Thomsen, M.,
1254 Goka, T., ... Koshiishi, H. (2008). A new international geostationary elec-

- 1255 tron model: Ige-2006, from 1 keV to 5.2 MeV. *Space Weather*, 6(7). doi:
1256 <https://doi.org/10.1029/2007SW000368>
- 1257 Sillanpää, I., Ganushkina, N. Y., Dubyagin, S., & Rodriguez, J. V. (2017). Electron
1258 fluxes at geostationary orbit from geosynchronous data. *Space Weather*, 15(12),
1259 1602-1614. doi: 10.1002/2017SW001698
- 1260 Simms, L. E., & Engebretson, M. (2020). Classifier neural network models predict
1261 relativistic electron events at geosynchronous orbit better than multiple re-
1262 gression or armax models. *Journal of Geophysical Research: Space Physics*,
1263 125(5), e2019JA027357. doi: <https://doi.org/10.1029/2019JA027357>
- 1264 Simms, L. E., Engebretson, M., Clilverd, M., Rodger, C., Lessard, M., Gjerloev, J.,
1265 & Reeves, G. (2018a). A distributed lag autoregressive model of geostationary
1266 relativistic electron fluxes: Comparing the influences of waves, seed and source
1267 electrons, and solar wind inputs. *Journal of Geophysical Research: Space*
1268 *Physics*, 123, 36463671. doi: <https://doi.org/10.1029/2017JA025002>
- 1269 Simms, L. E., Engebretson, M., & Reeves, G. (2022). Removing diurnal signals
1270 and longer term trends from electron flux and ulf correlations: a comparison
1271 of spectral subtraction, simple differencing, and arimax models. *Journal of*
1272 *Geophysical Research*.
- 1273 Simms, L. E., Engebretson, M. J., Clilverd, M. A., Rodger, C. J., & Reeves,
1274 G. D. (2018b). Nonlinear and synergistic effects of ulf pc5, vlf cho-
1275 rus, and emic waves on relativistic electron flux at geosynchronous orbit.
1276 *Journal of Geophysical Research: Space Physics*, 123(6), 4755-4766. doi:
1277 <https://doi.org/10.1029/2017JA025003>
- 1278 Simms, L. E., Engebretson, M. J., Pilipenko, V., Reeves, G. D., & Clilverd, M.
1279 (2016). Empirical predictive models of daily relativistic electron flux at
1280 geostationary orbit: Multiple regression analysis. *Journal of Geophysical*
1281 *Research: Space Physics*, 121(4), 3181-3197. doi: [https://doi.org/10.1002/](https://doi.org/10.1002/2016JA022414)
1282 [2016JA022414](https://doi.org/10.1002/2016JA022414)
- 1283 Simms, L. E., Engebretson, M. J., Rodger, C. J., Dimitrakoudis, S., Mann, I. R.,
1284 & Chi, P. J. (2021). The combined influence of lower band chorus and
1285 ulf waves on radiation belt electron fluxes at individual l-shells. *Jour-*
1286 *nal of Geophysical Research: Space Physics*, 126(e2020JA028755). doi:
1287 <https://doi.org/10.1029/2020JA028755>
- 1288 Simms, L. E., Pilipenko, V., Engebretson, M. J., Reeves, G. D., Smith, A. J., &
1289 Clilverd, M. (2014). Prediction of relativistic electron flux at geostationary
1290 orbit following storms: Multiple regression analysis. *Journal of Geophysical*
1291 *Research: Space Physics*, 119(9), 7297-7318. doi: [https://doi.org/10.1002/](https://doi.org/10.1002/2014JA019955)
1292 [2014JA019955](https://doi.org/10.1002/2014JA019955)
- 1293 Smith, G. (2018). Step away from stepwise. *Journal of Big Data*, 5(32). doi:
1294 <https://doi.org/10.1186/s40537-018-0143-6>
- 1295 Stepanov, N. A., Sergeev, V. A., Sormakov, D. A., Andreeva, V. A., Dubyagin,
1296 S. V., Ganushkina, N., & et al. (2021). Superthermal proton and electron
1297 fluxes in the plasma sheet transition region and their dependence on solar
1298 wind parameters), journal = Journal of Geophysical Research: Space Physics,
1299 volume = 126, e2020JA028580, doi = 10.1029/2020JA028580.
- 1300 Thomsen, M. (2004). Why *kp* is such a good measure of magnetospheric convection.
1301 *Space Weather*, 2, S11004. doi: 10.1029/2004SW000089
- 1302 Thomsen, M., Birn, J., Borovsky, J. E., Morzinski, K., McComas, D. J., & Reeves,
1303 G. D. (2001). Two-satellite observations of substorm injections at geosyn-
1304 chronous orbit. *Journal of Geophysical Research*, 106(A5), 8405-8416. doi:
1305 [10.1029/2000JA000080](https://doi.org/10.1029/2000JA000080)
- 1306 Thomsen, M., Henderson, M. G., & Jordanova, V. K. (2013). Statistical properties
1307 of the surface-charging environment at geosynchronous orbit. *Space Weather*,
1308 11(5), 237-244. doi: 10.1002/swe.20049
- 1309 Vette, J. (1991). *The AE-8 trapped electron model environment* (Tech. Rep.). Na-

1310
1311
1312
1313
1314
1315
1316
1317
1318
1319
1320
1321

- tional Aeronautics and Space Administration, Goddard Space Flight Center, Greenbelt, MD: National Space Science Data Center, World Data Center A for Rockets and Satellites.
- Whittingham, M., Stephens, P., Bradbury, R., & Freckleton, R. (2006). Why do we still use stepwise modelling in ecology and behaviour? *Journal of Animal Ecology*, 75(5), 11829. doi: 10.1111/j.1365-2656.2006.01141.x.
- Wing, S., Johnson, J. R., Turner, D. L., Ukhorskiy, A. Y., & Boyd, A. J. (2022). Untangling the solar wind and magnetospheric drivers of the radiation belt electrons. *Journal of Geophysical Research: Space Physics*. doi: 10.1029/2021JA030246
- Wright, S. (1934). The method of path coefficients. *Annals of Mathematical Statistics*, 5(3). doi: 10.1214/aoms/1177732676